Numerical Modeling of Hygrothermal : Chemical Transfer in Human Indoor Environment System

姜, 裕珍

Numerical Modeling of Hygrothermal – Chemical Transfer in Human Indoor Environment System

Yujin Kang

A thesis for the degree of

Doctor of Engineering

Department of Energy and Environmental Engineering

Interdisciplinary Graduate School of Engineering Sciences

Kyushu University

Japan

August 2020

THESIS SUMMARY

As indoor residence time increases, there is concern about the impact of indoor air quality (IAQ) on residents from the viewpoints of hygiene, health, and comfort. Especially, the influence of various pollutants existing in the indoor air on the health of the occupants is a very important issue in view of constant breathing and long exposure time.

The concentration distribution of air pollutants in the indoor environment is generally highly non-uniform because it is governed by nonlinear fluid phenomena. Based on CFD technology that can solve this problem, various numerical analysis models have been proposed to predict the concentration distribution of the indoor chemical. The models for chemical transport usually focus on the chemical advection/diffusion by fluid, the adsorption and desorption phenomena on the wall surface, the chemical reaction phenomena, and other physical elements. However, few studies have to discuss the interaction of each element in the transport of hygrothermal (heat and moisture) and chemicals.

From the point of view of analyzing the thermal environment and pollution level of indoor spaces, the numerical analysis usually focuses on predicting the risk of exposure to the human body. In this regard, it is necessary to analyze the change in the indoor environment due to the presence of human beings in indoor space, while the effects on the human body. Therefore, this research used the advanced computer simulated person (CSP), which can treat specific characteristics of the human body, for the CFD simulation.

This research focuses on analyzing the thermal environment and the pollutant level in the indoor space and around the human body based on detailed transport models that consider the interaction of each element in the hygrothermal and chemical transports.

The main objective of this research is the development of a numerical analysis model for hygrothermal and chemical transports in the human-indoor environment system in order to analyze indoor air quality and exposure risk of the human body, through three approaches:

i) approach to high-level models/methods for transport phenomena to increase the precision of numerical analysis; ii) approach to moisture and chemical transport phenomena by molecular diffusion environment system; iii) approach to hygrothermal and chemical transport phenomena by advection-diffusion in a human-indoor environment system.

This paper consists of five chapters, summarized below.

Chapter 1 summarizes the background and purpose of the study as an introduction. In particular, the numerical analysis model for predicting the concentration distribution for chemicals in the indoor environment is divided into the emission source model and the advection/diffusion model and discussed.

Chapter 2 outlines the governing equations such as turbulence models, heat transfer and radiation models, and scalar transport equations, which are the basis of the flow field, temperature field, humidity field, and contaminant concentration fields for the indoor environment analysis through CFD simulation. Moreover, the high-level models considered the interaction among thermal, humidity, and chemical, and detailed models contaminant emission were explained in this chapter.

Chapter 3 discusses the chemical transport phenomenon considering moisture diffusion in molecular diffusion dominated environment using a confined desiccator. By conducting a numerical analysis that reproduced the JIS desiccator method using the different desiccator, the usefulness of the detailed model for the emission from building materials and diffusion mechanisms of chemicals was confirmed, and the impact of the diffusion field geometry on the emission rates was predicted.

Chapter 4 describes the integrated analysis modeling for hygrothermal and chemical transport in the human-indoor environment system. The analysis model was created by integrating detailed models for fluid flow, hygrothermal, and chemical transports phenomena and a CSP integrated with the thermoregulation model. Moreover, by reproducing the ventilation and transfer of contaminants in the air gap between clothing and skin using a 3D scanning model of the actual clothing, the thermal, humidity, and contaminant concentration around the human body were quantitatively estimated, and the foundation data to establish a simplified numerical clothing model was obtained.

Chapter 5 summarizes the conclusions yielded by the present study and provides recommendations

for future works.

ACKNOWLEDGEMENTS

The present research, completed in 3 years at the Interdisciplinary Graduate School of Engineering Sciences, Kyushu University, would not have been possible without the assistance of many important people, to whom I wish to convey my sincere esteem and recognition.

I would like to express my sincere gratitude to my supervisor Professor Kazuhide Ito who gave me a new direction and continuous support during my research. I was able to do good research and have an opportunity to learn a lot because of his guidance. I respect him as a teacher and as a senior in life.

I would also like to extremely grateful for the committee members: Professor Takahito Miyazaki, Professor Daisuke Sumiyoshi, and Professor Naoki Ikegaya for their encouragement and insightful comments. I got valuable advice on all aspects of my research. I would like to thank Professor Kazuki Takenouchi for technical supports and advice for 3D digital modeling. I also want to extend my deepest thank you to Dr. Sung-Jun Yoo for his help and advice during my research and my study abroad life. His deep understanding of CFD simulation has provided fruitful discussions.

I would like to thank my colleague Mr. Kei Murota for his contributions to this research and also my appreciation for all former and current members of Ito Laboratory in the Department of Energy and Environmental Engineering, IGSES, Kyushu University. And Dr. Alicia María Murga Aquino, Dr. Nguyen Lu Phuong, and Dr. Juyeon Chung, your friendly help was a great pleasure for my study abroad life.

I would like to express my sincere gratitude to Professor Sumin Kim in the Department of Architecture and Architectural Engineering, Yonsei University, Korea. He guided me through the course of studying abroad in Japan through guidance from the master's program.

Finally, I dedicate my thesis to dear my mother. Her generosity and wisdom lead me on the right path, and she became a reliable supporter in my life. Thank you all the time. Thank you to my friends who have always cheered for me.

CONTENTS

CHAPTER 1

Introduction

1.1 Background

In modern societies, as people spend more than half of their life (70 to 90%) in various enclosed indoor spaces [1, 2], the control of indoor air quality (IAQ) and thermal environments which have a significant impact on the human physiological responses, sensations, and performance, have been pointed out. In this regard, much research on IAQ and thermal environment have been reported. Especially, many researchers have proposed a comprehensive estimation method based on numerical analysis techniques, including computational fluid dynamic (CFD), which is useful for estimating indoor environmental quality using coupled simulations through heat and mass transfer analysis [3-8]. Quantitative/qualitative analysis result from the numerical analysis allows a detailed estimation of IAQ and thermal environment, and this fruitful information has been commonly applied to the field of indoor environmental design [9].

For evaluating IAQ, there are many factors. Above all, long-term exposure to gaseous pollutants/chemicals such as radon, nitrogen dioxide, polycyclic aromatic hydrocarbons, formaldehyde, and volatile organic compounds (VOCs) can have a significant impact on human health. The concentration of these chemicals is exceedingly non-uniform affected by the nonlinear fluid phenomena in the indoor environment. To predict the indoor distribution of chemicals, numerical analysis models have been proposed based on CFD technology that can solve the nonlinear equation of fluids. Numerical analysis models of chemicals mainly cover convection and diffusion of chemicals, adsorption and desorption on walls, and chemical reactions. It is unusual for the study to have considered the interaction of each element in the transport of heat and moisture and the transport of chemicals.

Furthermore, it is necessary to analyze the effects on the human body as well as the changes in the indoor environment, accordance with the presence of human beings in the indoor space. An advanced

computer simulated person (CSP) capable of dealing with specific characteristics of the human body has been proposed for the CFD simulation [10, 11]. In addition, thermoregulatory function, breathing, dermal adsorption, and respiratory exposure mechanisms of contaminants, have been reproduced in detail [12-16]. By using these comprehensive human models, detailed health risks caused by poor IAQ and thermal environments as a result of interactions with the surrounding environment can be predicted [17, 18].

Against this background, the purpose of the research is the development of a numerical analysis model for hygrothermal (thermal and humidity) and chemical transports in the human–indoor environment.

In this study, the numerical analysis model for predicting the concentration distribution of chemical substances existing in the indoor environment is divided into the emission source model and the advection/diffusion model and discussed focusing on the numerical analysis method using fluid dynamics CFD:

i) approach to high-level models/methods for transport phenomena to increase the precision of numerical analysis; ii) approach to moisture and chemical transport phenomena by molecular diffusion environment system; iii) approach to hygrothermal and chemical transport phenomena by advection-diffusion in a human-indoor environment system.

Figure 1-1 shows the flow of the present study.

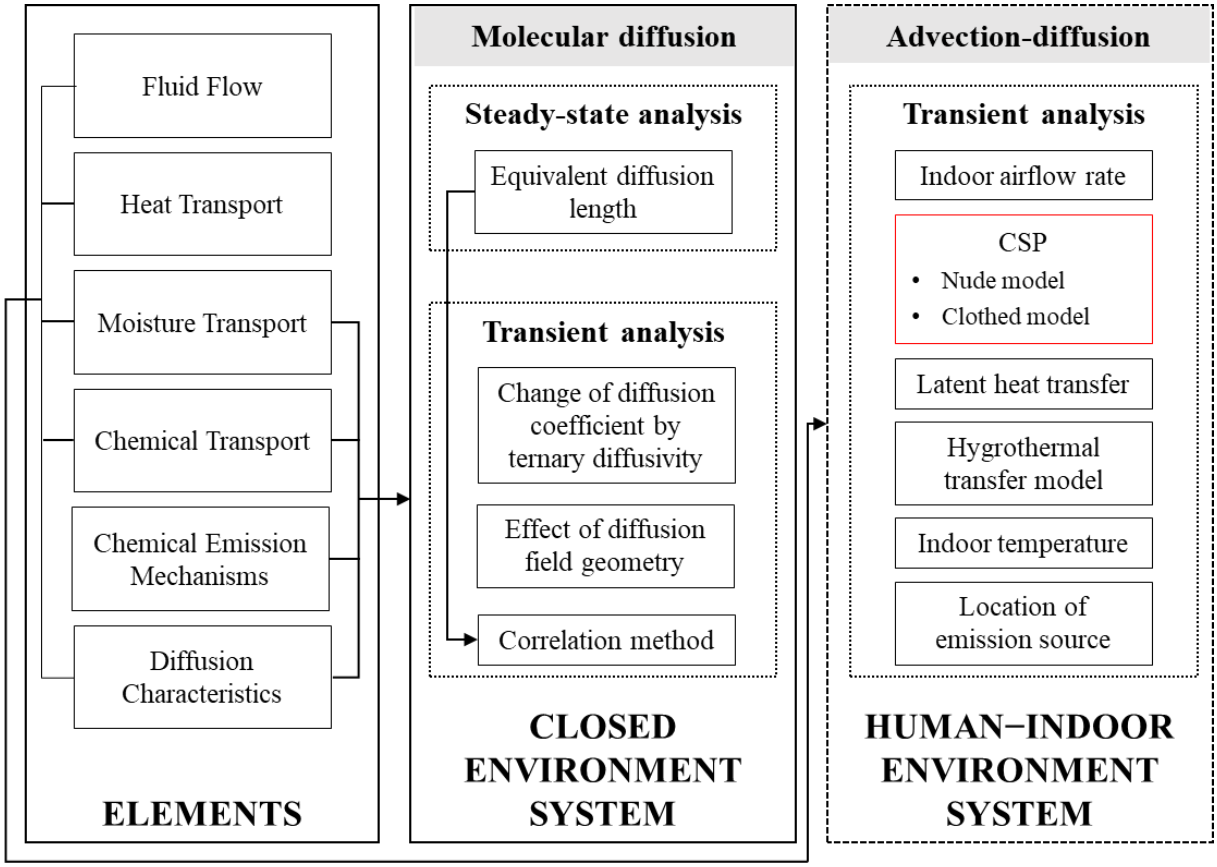

Figure 1-1. Schematic of the present study

1.2 Innovation to previous research

The transport of heat, moisture, and chemicals/pollutants generally exists in indoor environments and is an important factor in evaluating IAQ. In this regard, Zhang [19] proposed a system model to simulate the effect on indoor air quality by considering the interaction between several factors (heat, air, moisture, and pollutant). In this way, few studies have been conducted on the model of hygrothermal and chemical transport phenomena considering the interaction between elements. Form this point of view, the present study proposes a detailed transport phenomenon model by applying changes in the diffusivity of each element under molecular diffusion and advection-diffusion conditions and presents the analysis results using this model.

To clarify changes in the indoor environment when the human body is indoors, the CSP model applicable to CFD simulation has been developed by handling characteristics such as sensible heat and latent heat in the human body. In the CSP model, various thermoregulation models have been proposed that reproduce clothing that transfers heat generated from the human body, acting as a

protective barrier against heat and pollutants generated in the surrounding environment [20-24]. However, heat transfer through clothing is described in the model with simplification, generally as the resistance of sensible and latent heat transfer. A few studies suggest a comprehensive predictive method integrating a sophisticated and advanced hygrothermal and contaminant transfer model with the actual complex-structured clothes, but most of them often neglected specific impacts on heat/pollutant transport and certain influences on the surrounding flow field. Takada et al. [25] investigated air distribution and ventilation in the simple room located in the human body that considered the clothing geometry based on CFD simulation, but complex calculations such as hygrothermal transport and contaminant diffusion have not been performed. In this regard, the development of a clothing model and the application of hygrothermal and contaminant transfer between human and indoor environments based on CFD were proposed in the present research.

1.3 Objectives

The main objective of this research is to develop a numerical analysis model for the transport of hygrothermal (heat and moisture) and chemicals in the human-indoor environment system. Fluid flow, heat, moisture, and chemical transport phenomena were analyzed by CFD simulation, and the specific objectives can be derived as follows.

i. Observation of model/method to improve the accuracy of numerical analysis applying transport phenomenon models.
ii. Analyze the chemical transport phenomenon in a molecular diffusion environment system to predict the effects of diffusion field geometry.
iii. Development of an integrated numerical analysis model for analyzing the diffusion of hygrothermal and chemicals in an advection-diffusion environment.
iv. Prediction of change in the environment surrounding the human body based on reproduction actual clothing shape.

CHAPTER 2

Mechanisms of Fluid, Hygrothermal, and Chemical Transports

2.1 Foreword

This research aims to develop accurate numerical models considering the hygrothermal and chemical transports in the human-indoor environment. For fluid flow, hygrothermal, and chemical transports phenomena, a numerical model is reproduced based on computational fluid dynamics (CFD) simulation that can solve the nonlinear equation of fluid. Therefore, models for transport phenomena applied to the numerical analysis model are described in this chapter in this respect.

For the chemical, gaseous pollutants corresponding to substances generated by combustion, synthesis, decomposition of substances, or by physical properties were targeted. Based on the existing research on the causes and properties of these chemicals in the indoor environment, mathematical models applicable to numerical analysis for the emission mechanism and diffusion characteristics of chemicals were presented.

Governing equations of momentum, thermal energy, and scalar transport of each mathematical model are also hereby described.

2.2 Transport mechanisms in numerical analysis

CFD converts a nonlinear partial differential equation describing fluid phenomena into algebraic equations and solves fluid flow problems using algorithms of numerical techniques by a computer. To implement and analyze the transport phenomena of fluid, heat, moisture, and chemical in an indoor environment, this research uses ANSYS Fluent that is a commercial CFD analysis software.

2.2.1 Basic equations

Fluid flow phenomena are defined by the Navier-Stokes equations expressed in (2-1) and (2-2) for incompressible fluids.

$$\frac{\partial U_i}{\partial x_i} = 0 \tag{2-1}$$

$$\frac{\partial U_i}{\partial t} + U_j \frac{\partial U_i}{\partial x_j} = -\frac{1}{\rho} \cdot \frac{\partial P}{\partial x_i} + \nu \frac{\partial}{\partial x_j}\left(\frac{\partial U_i}{\partial x_j} + \frac{\partial U_j}{\partial x_i} \right) - g_i \beta \theta \tag{2-2}$$

Here, U_i represents wind speed (*u, v, w* components), ρ is the density, P is pressure, v is the kinematic viscosity coefficient, θ is the temperature (or the temperature difference from absolute zero, $\theta - \theta_0$), g_i is the gravity component of the acceleration vector in i direction, and β is the expansion coefficient. Continuity equation (2-1) indicates the density preservation law (mass conservation law) assuming constant density. The Navier-Stokes equation represented by equation (2-2) signifies the momentum law derived from Newton's second law and takes into account the effect of buoyancy.

For the non-isothermal flow field, equation (2-2) can be expressed by the thermal energy transport equation (2-3) as for the temperature field.

$$\frac{\partial \theta}{\partial t} + \frac{\partial U_j \theta}{\partial x_j} = \frac{\partial}{\partial x_j}\left(\alpha \frac{\partial \theta}{\partial x_j} \right) + S \tag{2-3}$$

Here, α is the thermal diffusion coefficient ($=\lambda/C_p \cdot \rho$), S is the heat generation term (heat source). This thermal energy transport equation (2-3) represents the energy conservation law and derived from Fourier's law.

Furthermore, as with the thermal energy transport equation (2-3), the moisture and chemical

transport phenomena can be defined by the scalar transport equation (2-4).

$$\frac{\partial \phi}{\partial t} + \frac{\partial U_j \phi}{\partial x_j} = \frac{\partial}{\partial x_j}\left(D \frac{\partial \phi}{\partial x_j} \right) + S' \tag{2-4}$$

Here, ϕ is the amount of scalars such as moisture and chemicals, and D is the diffusion coefficient of the target substance. By performing the coupled analysis of equations (2-1) to (2-4), it is possible to grasp the incompressible fluid and scalar transport phenomenon in the fluid.

2.2.2 Averaging the equation system

The series of equation systems from equations (2-1) to (2-4) are instantaneous physical quantities, and fluid phenomena can be completely grasped by solving these instantaneous equation systems directly. However, the Navier-Stokes equation (2-2) is impossible to solve by direct computation because of its complexity. Therefore, temporally and spatially consecutive physical quantities into finite ones by discretization, and then an analytical solution is derived by approximation. Discretizing the continuous quantity is equivalent to afford the calculated cut off frequency corresponding to the differential interval, and it is impossible to suppress the fluctuation of the physical quantity below the differential interval. In this respect, it is appropriate to apply the method of finding an approximate solution after averaging physical phenomena that occur below the difference interval.

The flow field analysis is performed using the ensemble average among various averaging operations. The ensemble average is expressed in equation (2-5).

$$\overline{f_k(x_i,t)}_E = \lim_{N\to\infty}\left(\frac{1}{N}\sum_{k=1}^{N} f_i(x,t) \right) \tag{2-5}$$

$$\overline{f(x_i)}_F = \int\int\int_{-\infty}^{\infty}\left(\prod_{i=1}^{3} G(x_i - x_i') \right) \cdot f(x_i')dx_i' \tag{2-6}$$

Here, the subscript E represents the ensemble average, and the subscript F represents the spatial average. In equation (2-6), the one-dimensional filter function $G(x_i)$ is imposed in three dimensions.

In equations (2-1) to (2-3), instantaneous values are separated into averages and fluctuations, and after applying the ensemble average the following equation can be obtained.

$$\frac{\partial \overline{U_i}}{\partial x_i} = 0 \tag{2-7}$$

$$\frac{\partial \overline{U_i}}{\partial t} + \overline{U_j} \cdot \frac{\partial \overline{U_i}}{\partial x_j} = -\frac{1}{\rho} \cdot \frac{\partial \overline{P}}{\partial x_i} + \nu \frac{\partial}{\partial x_j}\left(\frac{\partial \overline{U_i}}{\partial x_j} + \frac{\partial \overline{U_j}}{\partial x_i} \right) - \frac{\partial}{\partial x_j} \overline{u_i' u_j'} - g_i \beta \bar{\theta} \tag{2-8}$$

$$\frac{\partial \bar{\theta}}{\partial t} + \frac{\partial \overline{U_j} \bar{\theta}}{\partial x_j} = \frac{\partial}{\partial x_j}\left(\alpha \frac{\partial \bar{\theta}}{\partial x_j} \right) + \frac{\partial}{\partial x_j} \overline{u_j' \theta'} \tag{2-9}$$

Here, U_i, P, and θ are average values, and u_i', θ' are variation, and the overbar represents the ensemble average values. Equation (2-8) is called the Reynolds equation. Furthermore, the term $\overline{u_i' u_j'}$ in equation (2-8) is the Reynolds stress and $\overline{u_j' \theta}$ in equation (2-9) is the temperature flux. Originally, the definition of Reynolds stress is the concept of the product of density ρ and $\overline{u_i' u_j'}$; however, it has been simplified as only $\overline{u_i' u_j'}$.

2.2.3 Turbulence models

This section describes the low Reynolds number *k-ε* model of RANS (Reynolds Averaged Navier-Stokes) model. The standard *k-ε* model is generally a turbulence model for analyzing a flow field with a high Re number; however, the low Reynolds number *k-ε* model has been developed to improve these problems [26]. This model includes an attenuation function, f_μ, that takes into consideration the wall coordinate y^+ and the Reynolds number Rt when determining the viscosity coefficient V_t; the non-slip boundary condition in which the mech is sufficiently finely divided is applied in the region near the wall surface. In terms of the equation of the turbulence energy dissipation rate ε, the model function f_1 and f_2 are introduced in the production term and dissipation term of turbulence near the wall surface.

The basic equations for the low Reynolds k-ε model are as follows.

$$\frac{\partial \overline{U_i}}{\partial t} + \overline{U_j} \cdot \frac{\partial \overline{U_i}}{\partial x_j} = -\frac{1}{\rho} \cdot \frac{\partial \overline{P}}{\partial x_i} + \nu \frac{\partial}{\partial x_j}\left(\frac{\partial \overline{U_i}}{\partial x_j} + \frac{\partial \overline{U_j}}{\partial x_i} \right) - \frac{\partial}{\partial x_j} \overline{u_i' u_j'} \tag{2-10}$$

$$-\overline{u_i' u_j'} = \nu_t \left(\frac{\partial \overline{U_i}}{\partial x_j} + \frac{\partial \overline{U_j}}{\partial x_i} \right) - \frac{2}{3} k \delta_{ij} \tag{2-11}$$

$$\nu_t = C_\mu \cdot f_\mu \cdot \frac{k^2}{\varepsilon} \tag{2-12}$$

$$\frac{\partial k}{\partial t} + \overline{U}_j \frac{\partial k}{\partial x_j} = D_k + P_k - \left(\bar{\varepsilon} + D \right) \tag{2-13}$$

$$\frac{\partial \bar{\varepsilon}}{\partial t} + \overline{U}_j \frac{\partial \bar{\varepsilon}}{\partial x_j} = D_\varepsilon + \frac{\bar{\varepsilon}}{k} \cdot \left(C_{\varepsilon 1} \cdot f_1 \cdot P_k - C_{\varepsilon 2} \cdot f_2 \cdot \bar{\varepsilon} \right) + E \tag{2-14}$$

$$P_k = -\overline{u_i' u_j'} \cdot \frac{\partial \overline{U}_i}{\partial x_j} \tag{2-15}$$

$$D_k = \frac{\partial}{\partial x_j} \cdot \left(\left(\nu + \frac{\nu_t}{\sigma_k} \right) \frac{\partial k}{\partial x_j} \right) \tag{2-16}$$

$$D_\varepsilon = \frac{\partial}{\partial x_j} \cdot \left(\left(\nu + \frac{\nu_t}{\sigma_\varepsilon} \right) \frac{\partial \bar{\varepsilon}}{\partial x_j} \right) \tag{2-17}$$

$$\bar{\varepsilon} = \varepsilon - 2\nu \left(\frac{\partial \sqrt{k}}{\partial x_k} \right)^2 \tag{2-18}$$

Here, f_μ, f_1, and f_2 represent model functions, D and E have been introduced when $\bar{\varepsilon}$ is used.

In the low Reynolds k-ε model, the model function (equation (2-12)) that is generally calculated using the wall coordinate y^+ is applied; however, in the case of y^+, there are many models with $f_\mu = 0$ in the region where the wall friction velocity $u_\tau = 0$, and the viscosity coefficient is established to $\nu_\tau = 0$ in this case. This case is an irrational phenomenon physically. Therefore, the Abe-Kondoh-Nagano model can be applied to flow field analysis in which redeposition and separation phenomena occur by introducing the Kolmogorov velocity scale instead of y^+ and using a new parameter y^*.

The model functions and numerical constants of the Abe-Kondoh-Nagano model are summarized as follows.

$$f_\mu = \left\{ 1 - \exp\left(-\frac{y^*}{14} \right) \right\}^2 \left[1 + \frac{5}{R_t^{3/4}} \cdot \exp\left\{ \left(\frac{R_t}{200} \right)^2 \right\} \right] \tag{2-19}$$

$$f_1 = 1.0 \tag{2-20}$$

$$f_2 = \left\{1 - \exp\left(-\frac{y^*}{3.1}\right)\right\}^2 \left[1 - 0.3 \cdot \exp\left\{-\left(\frac{R_t}{6.5}\right)^2\right\}\right] \tag{2-21}$$

$$\bar{\varepsilon} = \varepsilon = 2\nu\left(\frac{\partial\sqrt{k}}{\partial y}\right)^2 \tag{2-22}$$

$$R_t = \frac{k^2}{\nu\varepsilon} \tag{2-23}$$

$$y^* = \frac{u_\varepsilon y}{\nu} = \frac{y}{\eta} \tag{2-24}$$

$$\eta = \frac{\nu^{3/4}}{\varepsilon^{1/4}} \tag{2-25}$$

$$u_\varepsilon = (\nu\varepsilon)^{1/4} \tag{2-26}$$

Here, equation (2-22) expresses the wall boundary condition of ε; η is the Kolmogorov length scale in equation (2-25), and u_ε is the Kolmogorov velocity scale in equation (2-26). In the previous equations $C_\mu = 0.09$, $C_{\varepsilon 1} = 1.5$, $C_{\varepsilon 2} = 1.9$, $\sigma_k = 1.4$, $\sigma_\varepsilon = 1.4$, and $D = E = 0$.

2.2.4 Radiation model

The model of surface-to-surface (S2S) is a radiation analysis model used in the commercial CFD code ANSYS FLUENT to define the radiation exchange in an enclosure of a gray diffuse surface. In this model, the radiant energy exchange between two surfaces depends on dimensions of the surface, the distance between surfaces, and lateral direction, and these parameters are defined by a view factor. In addition, this S2S model assumes that the effects of absorption, reflection, and scattering of radiation in space are ignored; therefore, only the effect of radiation between surfaces is considered in the analysis using the S2S radiation model.

The S2S model assumes that emissivity and absorption are equivalent ($\varepsilon = \alpha$) in accordance with Kirchhoff's law and that reflectance of the diffuse surface is independent of the reflection (or incident) direction. It is also applicable for indoor ventilation analysis to using very low computational resources [27].

The energy flux leaving the surface k is composed of directly emitted and reflected energy and can be expressed by the following equation.

$$q_{out,k} = \varepsilon_k \sigma T_k^4 + \rho_k q_{in,k} \tag{2-27}$$

Here, $q_{out,k}$ is the energy flux leaving the surface, ε_k is the emissivity, σ is the Stefan-Boltzmann constant, ρ_k is the density, and $q_{in,k}$ is incident flux on surface k from the surroundings.

The incident energy from one surface to another depends directly on the view factor F_{jk} in the S2S model. The view factor F_{jk} is the ratio of energy leaving surface j and incident on surface k. The incident energy flux $q_{in,k}$ can be expressed as the energy flux leaving surfaces by the following equation.

$$A_k q_{in,k} = \sum_{j=1}^{N} A_j q_{out,k} F_{j,k} \tag{2-28}$$

Here, A_k is the area of surface k, and F_{jk} is the view factor when the surface k is viewed from the surface j. Applying the correlation of the shape coefficients on N surfaces is the following equation.

$$A_j F_{jk} = A_k F_{kj} \quad (j = 1, 2, 3, \ldots, \mathrm{N}) \tag{2-29}$$

Then the following equations (2-30) and (2-31) are obtained.

$$q_{in,k} = \sum_{j=1}^{N} F_{jk} q_{out,j} \tag{2-30}$$

$$q_{out,k} = \varepsilon_k \sigma T_k^4 + \rho_k \sum_{j=1}^{N} F_{jk} q_{out,j} \tag{2-31}$$

Finally, the equation can be expressed as equation (2-32).

$$J_k = E_k + \rho_k \sum_{j=1}^{N} F_{jk} J_j \tag{2-32}$$

Here, J_k is the radiosity, and E_k is the emissive power. This equation can be recast into a matrix form as follows.

$$KJ = E \tag{2-33}$$

Here, K is the $N \times N$ matrix, J is the radiosity vector, and E is the radiation power vector. Surface cluster temperature can be calculated by area averaging by using the radiosity matrix equation (2-33).

$$T_{SC} = \left(\frac{\sum_f A_f T_f^4}{\sum A_f} \right)^{1/4} \tag{2-34}$$

Here, T_{SC} is the temperature, and A_f and T_f are the area and temperature of the face, respectively.

2.2.5 Scalar transport

Reproducing the transport phenomena of chemicals emitted indoors, simultaneously with the moisture transport phenomenon, is an important task in this research. Moisture and chemicals are assumed to be passive scalars, and calculated by the scalar transport equation (2-35).

$$\frac{\partial \bar{\phi}}{\partial t} + \frac{\partial \overline{U_i}\,\bar{\phi}}{\partial x_i} = \frac{\partial}{\partial x_i}\left\{ \left(D + \frac{\nu_t}{\sigma} \right) \frac{\partial \bar{\phi}}{\partial x_i} \right\} \tag{2-35}$$

Equation (2-35) shows the equation of gradient diffusion approximation to the transport equation of the scalar quantity shown in equation (2-4).

2.2.6 Mass flux and flux conservation

Flux describes the rate at which a specific physical quantity is transported per unit time through a unit area perpendicular to a given direction. In transport phenomena research, many different types of fluxes are used, each with its distinct unit of measurement along with distinct physical constants.

Among them, mass flux represents the mass flow rate across a unit area and can be expressed as the equation (2-36).

$$flux_m = \frac{\dot{m}}{A} = \rho \cdot v_n \tag{2-36}$$

Here, $flux_m$ [kg m^{-2} s^{-1}] is mass flux, $\dot{m}$ [kg s^{-1}] is the mass flow rate, A [m^2] is cross-sectional vector area/surface, and v_n [m s^{-1}] is flow velocity of the mass elements. The mass flux can also refer to an alternate form of flux in Fick's law that includes the molecular mass (eq. (2-37)).

$$flux_m = -D \frac{d\varphi}{dx} \tag{2-37}$$

Here, D [m^2 s^{-1}] is the diffusion coefficient, φ [kg m^{-3}] is the concentration for ideal mixture, and

x [m] is position.

When a substance passes through any surface, the mass flux of substance for that surface should be constant according to the conservation law. In the case of moving to different phases through the surface, a unit conversion of the concentration for substance is necessary. Accordingly, the present research converts the concentration unit of a substance by using the partition coefficient concept (P).

2.2.7 Hygrothermal transport model

To determine the transfer of heat and moisture in the solid phase, the hygrothermal transport equation is solved using the basic equation of simultaneous heat and moisture transport, assuming that the solid phase is hygroscopic. Equations (4-1) and (4-2) show the hygrothermal transport equations for each heat and moisture [28].

$$(C_s\rho_s + Lv)\frac{\partial T}{\partial t} = \frac{\partial}{\partial x_i}\left(\lambda_T \frac{\partial T}{\partial x_i}\right) + L\kappa\frac{\partial X}{\partial t} \tag{2-38}$$

$$\left(k\rho_s + \kappa\right)\frac{\partial X}{\partial t} = \frac{\partial}{\partial x_i}\left(\lambda_X \frac{\partial X}{\partial x_i}\right) + \nu\frac{\partial T}{\partial t} \tag{2-39}$$

Here, C_s [W s kg^{-1} K^{-1}] is the specific heat capacity, L [W s kg^{-1}] is the heat of condensation, $_V$ [kg m^{-3} K^{-1}] is the water content change for temperature change, $_K$ [kg m^{-3} (kg/kg')$^{-1}$] is the water content change for absolute humidity change, and k [-] is the porosity of clothes, while λ_T [W m^{-1} K^{-1}] and λ_X [W m^{-1} (kg/kg')$^{-1}$] represent the thermal and moisture conductivity of clothes.

2.3 Characteristics of chemical transport

By considering the mechanisms for the emission and diffusion characteristics of chemicals in the numerical analysis model, the analysis accuracy of the chemical transport phenomenon is improved.

2.3.1 Emission mechanisms from building materials

Building materials are the main cause of indoor pollutants, that is, they are the emitted source for chemicals in the indoor environment. The emission of chemicals in these building materials can be divided into two categories: external (evaporative) diffusion control type and inner diffusion control type.

The external (evaporative) diffusion type materials assume that the emission concentration on the building material surface is constant, as the diffusion resistance in the interior of the material is extremely tiny. This building material manifests a slight resistance to mass transfer defined by the effective diffusion coefficient and relatively high resistance to convective mass transfer [29]. In the case of targeting the building materials of the external (evaporative) diffusion control type, the emission rate, flux of the emission surface, is greatly affected by the concentration distribution characteristics in the air [30].

The Inner diffusion control type, that the effective diffusion coefficient in the building material is considerably smaller than the molecular diffusivity in the air, can be to assume that the emission flux on the material surface is almost constant without depending on the concentration distribution in the air [30-34].

Wood-based panels are generally categorized as the building material of the inner diffusion control type. It was confirmed that emissions of formaldehyde and VOCs from building materials are generally internal diffusion-controlled accordance with emissions model studied and some follow-up studies by Little et al [35]. On the other hand, one of the pioneering studies on the modeling of emissions from building materials reported that the emission characteristics of building material such as plywood and fiberboard are modeled using equilibrium surface concentration and classified as the

external or evaporative diffusion control types [36]. Therefore, the emission mechanism from building materials is highly dependent on the control type and there are still various modeling possibilities for determining emission characteristics, including internal and external diffusion mechanisms.

2.2.2 Diffusion coefficient of chemicals

The diffusion coefficient is a proportionality constant between diffusion flux and concentration gradient and depends on the temperature, pressure, and properties of the target substance such as molecule size. Furthermore, the diffusion coefficient in gas and liquid phases differ, due to the different number density of molecules and mobility, in each phase; e.g., the diffusion coefficient of a compound in the air is approximately 1000 times the diffusion coefficient in water. Therefore, this study describes the equations for calculating the diffusion coefficient dependent on temperature in gas and liquid d phases.

2.2.2.1 Diffusion coefficient in the gas phase

The dependence of the diffusion coefficient on the temperature in the gas phase can be expressed using the Chapman-Enskog equation from equation (2-38).

$$D_{AB} = \frac{A \cdot T^{3/2} \cdot \sqrt{1/M_A + 1/M_B}}{p \cdot \sigma_{AB}^2 \cdot \Omega} \tag{2-40}$$

Here, D_{AB} [$m^2\ s^{-1}$] is a binary diffusion coefficient of component A and B, A [atm Å cm^2 $(g\ mol)^{1/2}$ $K^{-3/2}\ s^{-1}$] is an empirical coefficient (=1.8583×10^{-7}), T [K] is the temperature, M_A [$g\ mol^{-1}$] is the molar mass of component A, p [atm] is the pressure, σ_{AB} [Å] is the average collision diameter (= $(\sigma_A + \sigma_B)/2$), and Ω [-] is a temperature-dependent collision integral. This equation calculates the molecular diffusion coefficient of a substance on the assumption that there is only one substance (component B) in the dry gas phase (component B).

In the indoor air, moisture or other substances are present in the gas phase, which can affect the

diffusion of the substances. Therefore, a multi-component diffusion coefficient based on the Wilke equation (2-39), which was derived from the theories of Maxwell and Stefan [37, 38], is presented for precise molecular diffusion calculation.

$$D'_A = \frac{1 - Y_A}{Y_B / D_{AB} + Y_C / D_{AC} + \cdots} \tag{2-41}$$

Here, D'_A [m^2 s^{-1}] is an effective diffusion coefficient of component A, and Y_A [-] is the mole fraction of component A. The mole fraction is determined by the number of moles calculated according to the concentration of each component, i.e., the diffusion coefficient of chemical in a mixed gas is influenced by the concentration.

2.2.2.2 Diffusion coefficient in the liquid phase

The diffusion coefficient of formaldehyde in a liquid is calculated by using the Stoke-Einstein equation expressed in (2-40).

$$D_A = \frac{k_B \cdot T}{6\pi \cdot \mu \cdot R_0} \tag{2-42}$$

Here, D_A [m^2 s^{-1}] is the diffusion coefficient in liquid, k_B [m^2 kg s^{-2} K^{-1}] is Boltzmann's constant (= 1.380×10^{-23}), μ [kg m^{-1} s^{-1}] is dynamic viscosity, R_0 [m] is the radius of the spherical particle.

CHAPTER 3

Chemical Transport in Confined Small Glass Desiccator

3.1 Foreword

For measuring the chemical emission rates from building materials and products, a variety of methods can be found in international/national standards. The chamber method, prescribed in ISO 16000-9 [39], is the standard recommended method for measuring emission rates of volatile organic compounds (VOCs), one of the chemicals that is an evaluation factor of indoor air quality, in building materials and products. This method is a dynamic method in which fresh air is continuously and constantly supplied to the chamber; therefore, it uses a scaled-down simulation of the general indoor environment, with the air supply and exhaust corresponding to actual room ventilation conditions [40, 41]. Moreover, the static method, e.g., the headspace method, has widely been used as an alternative to the dynamic method. In a static method, the process first established equilibrium of the VOC concentration in an enclosed airtight space and then analyzes this equilibrium concentration through active or passive sampling. This static method may be affected by experimental conditions such as chamber size and geometry, the relative position of the test specimen and sorbent, and or test duration.

In this section, the target chemical is formaldehyde as a representative substance among indoor pollutants. Therefore, this section focuses on formaldehyde emission testing in small confined desiccators, prescribed as JIS A 1460 [42], which is frequently used as an alternative screening method to the dynamic method, in Japan.

Against this background, to analyze the effect of the emission mechanisms from building material summarized in Chapter 2 and of the change of diffusion filed, this chapter describes the chemical transport phenomena by molecular diffusion in a confined environment system using a small glass desiccator. At this time, the change of molecular diffusion coefficient of chemical due to the transport phenomenon of moisture was considered. In this study, the target chemical is representative formaldehyde among indoor pollutants.

3.2 Methodology

3.2.1 Desiccator method

The desiccator method specified in ISO/DIN 12460-4 (or JIS A 1460) [42, 43] is used to determine the amount of formaldehyde emitted from particleboard, fibreboard, plywood, oriented strand board, and wooden laminated flooring. This method has a procedure similar to that of the static headspace analysis where formaldehyde emitting material and water sorbent are installed in a closed vessel. The formaldehyde emitted from the building materials is absorbed in water (absorbent) for 24 h, and the volume-averaged concentration in the water is measured to determine the formaldehyde releases from the building materials. This desiccator method can measure formaldehyde emission more simply and quickly compared with dynamic chamber methods, and it is widely used as a simple screening method.

Risholm-Sundman et al. [44] compared commonly used European test methods including chamber, gas analysis, flask, perforator, and Japanese test including desiccator and small chamber methods for solid wood, particleboard, plywood and medium-density fibreboard (MDF). Kim et al. [45]concluded that desiccator and perforator methods produced proportionally equivalent results where the reproducibility of testing formaldehyde and total VOC emissions from wood-based composites and engineered flooring by using a desiccator, a perforator, and a 20L small chamber are assessed. The correlation between formaldehyde levels recorded by using the chamber and desiccator methods was observed by Que and Furuno [46]. Que et al. [47] demonstrated the utility of the Japanese desiccator method for measuring formaldehyde emission from particleboard and MDF. Furthermore, where building materials of the same thickness and type are used for the formaldehyde emission test, the correlations between the results obtained by the desiccator and chamber (dynamic) methods have been discussed, according to Böhm et al. [48].

Based on the JIS standard, the test of the desiccator method was performed by measuring the amount absorbed on 300 mL of water in a sealed desiccator installed the formaldehyde emission source of 10 specimens, for 24 h under an isothermal condition of 20 °C. Figure 3-1 shows the experimental setup for measuring the formaldehyde emission rates using desiccator. After the 24-h

period of the test, the formaldehyde concentration sorbed on the water is quantitatively determined by acetylacetone molecular sorption spectrophotometry, based on the Hachsch reaction in which formaldehyde absorbed in water reacts with ammonium ions and acetylacetone to produce diacetyl-dihydrolutidine (unit: mg/L) [42].

Figure 3-1. Photographs of the experimental setup for formaldehyde emission rates

3.2.2 Small glass desiccator

To clarify the impact of diffusion field changes by chamber size and geometry on chemical transport, this study procured five types of small glass desiccators with low formaldehyde adsorption. Table 3-1 shows a list of targeted glass desiccators. Type R is a desiccator used in a method for measuring formaldehyde emission rates specified in JIS (Japanese Industrial Standard) A 1460 in Japan. To confirm the impact of desiccator geometry on formaldehyde emissions from building materials, four types of small glass desiccator are prepared, which are prescribed in ISO (International Organization for Standardization) and DIN (Deutsches Institut für Normung) standards of different manufacturers (Type A, B, C, and D). The appearance of Type R is different from the other desiccator since it has an indentation shape at the bottom to hold the sorbent. Type A, B, and D seemed similar, and it was difficult to visually confirm any significant variation in geometry. Type C appeared to be significantly shorter than the other desiccators. In addition, two units of each desiccator type were prepared to account for any manufacturing deviation.

Table 3-1. List of small glass desiccators

Desiccator	Type R (R-1, R-2)	Type A (A-1, A-2)	Type B (B-1, B-2)	Type C (C-1, C-2)	Type D (D-1, D-2)
Manufacturer	ISAMI Co., Ltd (Japan)	BRAND Co., Ltd (Germany)	SIMAX Co., Ltd (Czech)	ISO LAB Co., Ltd (Germany)	CORNING Co., Ltd (USA)
Reference Standard	JIS R 3503	DIN 12491	ISO 13130	DIN 12491 ISO 13130	-
The diameter of the partition panel [mm]	240	235	239	240	230
Size [mm]	Int. diameter: 240 Height: 380 (max) ± 20	Ext. diameter: 320 Height: 357	Ext. diameter: 320 Height: 363	Int. diameter: 329 Height: 325	Int. diameter: 274 Height: 357
Material	1) Borosilicate glass – I 2) Borosilicate glass – II 3) Soda-lime glass	Borosilicate glass 3.3 DIN ISO 3585	Borosilicate glass 3.3 DIN ISO 3585	Borosilicate glass 3.3 DIN ISO 3585	Borosilicate glass ASTM E438-92 Type I, Class A

3.2.3 Formaldehyde emission test

To estimate the amount of emission on building materials surface and ensure the validation and verification of the analytical data, the formaldehyde emission tests were conducted using the different two types of desiccator (Type R and Type A). The examination of formaldehyde emissions of round robin tests was conducted at five Japanese institutions. Besides, the formaldehyde emission test used two types of building materials (MDF): high- and low-emission material corresponding to F-Two star and F-Four star by Japanese Industrial Standard (JIS), respectively. The MDF is generally categorized as a building material of the inner diffusion control type regarding formaldehyde emission. The constant emission flux value of building material surfaces relevant to the boundary condition of the numerical analyses, therefore, is estimated by this test.

Table 3-2 shows the experimental results of the formaldehyde emission test for five different desiccators [49]. The difference in average formaldehyde concentration in water after 24 hours for the two types of desiccator was less than 1% for low-emission building material; whereas, in the case of the high-emission material, the difference was approximately 5%. Based on the experimental results, the time-averaged formaldehyde emission rates from building materials were estimated by using the flux conservation equation (Table 3-3).

Table 3-2. Experimental results for the formaldehyde emission test

The emission level of building material / Desiccator type		Low-emission		High-emission	
		Type R-1 Type R-2	Type A-1 Type A-2	Type R-1 Type R-2	Type A-1 Type A-2
Formaldehyde concentration in water [mg/L]	1	0.14 0.14	0.13 0.13	1.03 1.02	1.02 1.00
	2	0.15 0.13	0.13 0.16	1.11 1.01	0.93 1.03
	3	0.13 0.11	0.11 0.14	0.84 0.84	0.81 0.83
	4	0.124 0.14	0.136 0.138	1.018 0.958	0.89 0.943
	5	0.16 0.14	0.14 0.14	0.87 0.87	0.81 0.83
	Avg	0.14	0.14	0.96	0.91
Standard deviation (STD)		0.01	0.01	0.08	0.09

3.2.4 Three-dimensional digital modeling

For the numerical analyses, the three-dimensional (3D) digital models were generated: the internal geometry of targeted five desiccators was modeled by using a laser 3D scanner (EXAscan, CREAFORM) with the high precision of scan data (approximately ± 0.055 mm), and ten sections of building material and a crystal petri dish were formed inside. Here, building materials are hypothetical formaldehyde emission sources with a constant emission rate/concentration for numerical analysis, and each section consists of an area 180 cm^2 with 150 mm length and 50 mm width as specified in the formaldehyde emission test (JIS A 1460). The crystal dish with 115 mm in inner diameter and 60 mm in depth was installed in the bottle of the desiccator, and contained 300 ml of de-ionized water, which acts as an absorbent for formaldehyde capture. The 3D digital models were created with tetrahedral mesh. Ten prism mesh layers were created at the vicinities of the building materials and water surface, to precise the emission and adsorption phenomenon for each surface. Grid independence was carefully checked. Figure 3-2 shows the 3D models of five desiccators. The detailed data for each desiccator model based on the 3D models is presented in Table 3-3. The size was measured at the points stipulated in ISO 13130 [50], as shown in Figure 3-2(f).

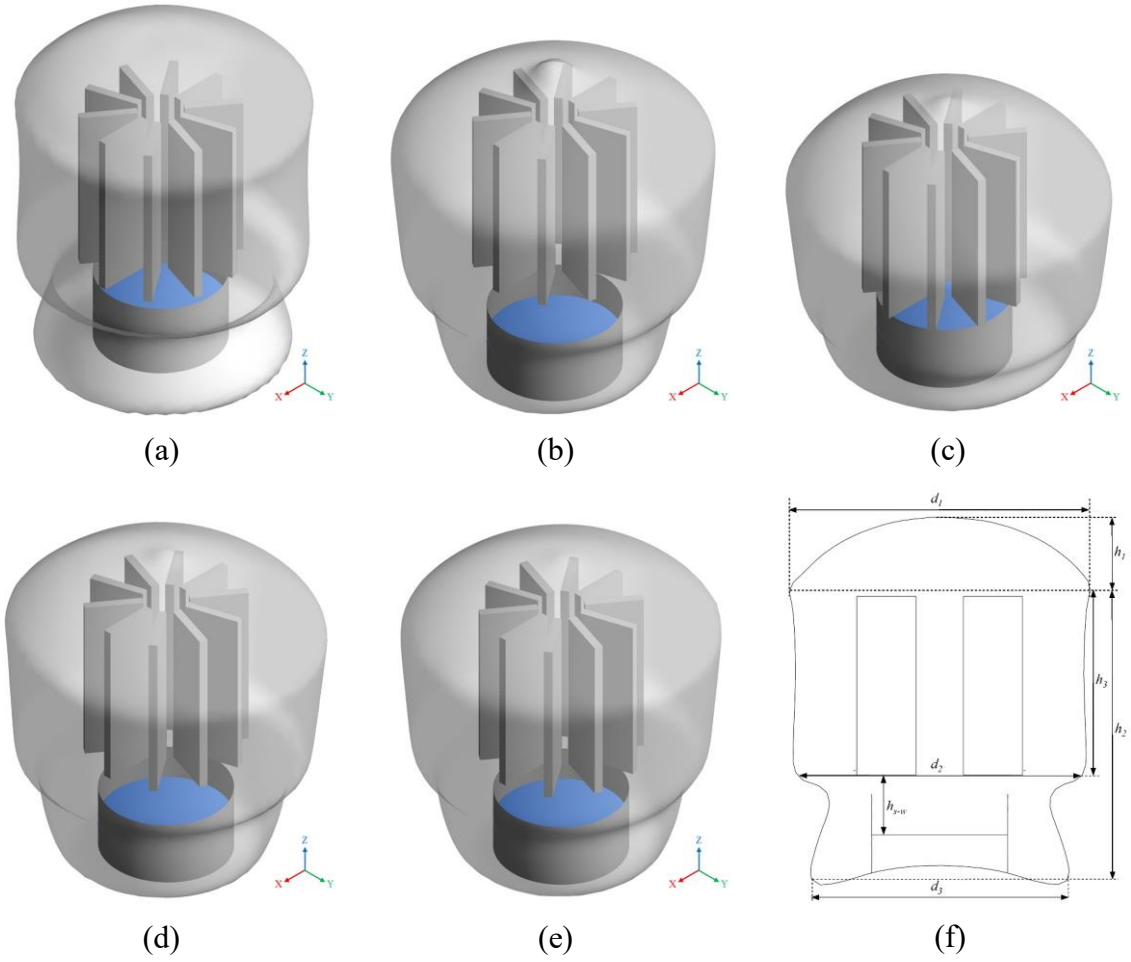

Figure 3-2. 3D modeling of five desiccators: (a) Type R, (b) Type A, (c) Type B, (d) Type C, (e) Type D, and (f) Desiccator measurement points using Type R as prescribed in ISO 13130

Table 3-3. Detail data of the 3D models of desiccator

Desiccator		Type R		Type A		Type B		Type C		Type D	
		R-1	R-2	A-1	A-2	B-1	B-2	C-1	C-2	D-1	D-2
Tetrahedral meshes		803 086	801 910	809 313	807 736	805 149	808 217	794 495	802 398	811 071	815 723
Volume [m^3]		0.01145	0.01174	0.01163	0.01168	0.01171	0.01155	0.01038	0.01033	0.01168	0.01164
Vertical distance, h_{s-w} [mm]		50	45	75	72	79	80	39	39	70	69
Size at the points [mm]	d_1	254	254	272	272	274	276	276	275	271	271
	d_2	236	241	250	246	249	251	252	251	242	241
	d_3	219	213	170	169	165	170	196	193	166	167
	h_1	253	254	218	219	219	217	158	160	219	217
	h_2	58	61	77	73	87	88	96	109	78	74
	h_3	161	166	129	128	122	119	101	102	135	131

3.2.5 Outline numerical analysis

To clarify the transient formation of the formaldehyde concentration distribution in the confined desiccators, both steady-state and transient analyses were conducted to clarify the formaldehyde emission from building materials, diffusion, and adsorption into the water in different five desiccators generated with 3D digital models. The steady-state analysis was performed to estimate an equivalent diffusion length, L_d, by the emission rate under perfect sink condition. The non-uniform distribution of formaldehyde concentration over the 24-hour test was investigated by the transient analysis. Formaldehyde in the desiccator is emitted from building material and diffuses and sorbs to the water surface installed at the low part of the desiccator. Equation (3-1) shows the governing equation for formaldehyde diffusion in the confined desiccator.

$$\frac{\partial C}{\partial t} = \frac{\partial}{\partial x_j}\left(D \frac{\partial C}{\partial x_j} \right) \tag{3-1}$$

Table 3-4 shows the boundary conditions for both the steady-state and transient analyses. The walls of the desiccator and petri dish were assumed that formaldehyde was not adsorbed on the surface. In this study, the diffusion coefficient was calculated under atmospheric pressure conditions at the test temperature of 20 °C.

Table 3-4. Conditions of numerical analysis

Method			Steady-state	Transient A	Transient B	
					High-	Low-
Boundary conditions	Desiccator and Petri dish walls		Gradient zero	Gradient zero	Gradient zero	Gradient zero
	Building material (emission mechanism)		$C_s = 1$ (External diffusion)	C_s = 900 μg/kg$_a$ (External diffusion)	$flux_s$ = 0.0185 ug/m^{2}s (Inner diffusion)	$flux_s$ = 0.0026 ug/m^{2}s (Inner diffusion)
	Water surface	Formaldehyde	$C_s = 0$ (Perfect sink hypothesis)	$flux_a = flux_w$ (Flux conservation)	$flux_a = flux_w$ (Flux conservation)	$flux_a = flux_w$ (Flux conservation)
		Water vapor	-	$X_s = 0.6198 \times (p_{ws} / (p_a - p_{ws}))$	$X_s = 0.6198 \times (p_{ws} / (p_a - p_{ws}))$	$X_s = 0.6198 \times (p_{ws} / (p_a - p_{ws}))$
Diffusion coefficient	Air phase		$D_a = 13.6 \times 10^{-6}$ m^2/s (Binary diffusivity)	Defined as ternary diffusivity	Defined as ternary diffusivity	Defined as ternary diffusivity
	Water phase		-	$D_w = 0.18 \times 10^{-6}$ m^2/s	$D_w = 0.18 \times 10^{-6}$ m^2/s	$D_w = 0.18 \times 10^{-6}$ m^2/s

At for the desiccator method, the order of adsorption onto the glass surface is confirmed to be much smaller than that of adsorption/dissolution or trapping to the water because water is used as an adsorbent in terms of the hydrophilic characteristics of formaldehyde. Future, the time that formaldehyde concentration in the air phase of desiccator reaches equilibrium is assumed to be shorter than the 24 h of test time, and adsorption equilibrium is established quickly on the glass wall surfaces in the steady-state condition. In the numerical analyses, From these assumptions, the impact of the adsorption effect on the glass of desiccator on the formaldehyde concentration distribution and volume-averaged concentration in the water is considered to be insignificant.

3.2.5.1 Steady-state analysis and equivalent diffusion length

The substantive diffusion length from the building material surface to the water surface varies between different desiccator geometry and the positioning of the emission and sorption materials. To clarify this diffusion length, equivalent diffusion length, namely L_d, was calculated by steady-state analysis. The boundary conditions in the steady-state analysis were assumed, as shown in Table 3-4. When assuming a linear-type (Henry type) sorption isotherm, the surface concentration of $C_S = 0$ on the water surface coincided with the assumptions of the perfect sink hypothesis and Henry constant, $kh = \infty$; therefore, the boundary condition of the water surface is assumed concentration zero. In the steady-state analysis, the formaldehyde emission material is assumed of external diffusion control type, and the emission surface concentration is given $C_S = 1$ corresponding to the dimensionless concentration, as Dirichlet boundary condition (that is referred to as a fixed boundary condition). The L_d is calculated as the quantum of emission flux, $flux_m$, for each desiccator obtained by this analysis.

The external diffusion type of building material is affected by the concentration distribution characteristics in the air as described in *Chapter 2*. The equation for calculating mass flux (equation (2-37)) can be rendered discrete by assuming a simplistic hypothetical condition in which both the normalized surface concentration of the building material and that of water as with the conditions of steady-state analysis. These conditions are shown in equation (3-2).

$$flux_m = -D\frac{0-1}{L_d} = D\frac{1}{L_d} \quad (3\text{-}2)$$

Here, L_d indicates the average diffusion length [m], which defined as the equivalent diffusion length, from the building material surface to the water surface. As shown in the equation, the $flux_m$ depends directly on L_d, its value represents the comparable length scale for diffusion in the confined space with a complicated geometry under fixed concentration difference conditions.

3.2.5.2 Transient analysis

The objective of the transient analyses was to determine the non-uniform formaldehyde concentration distribution in air and water in the confined desiccator. For the emission surface, the boundary conditions assumed two cases for building materials of the external and inner diffusion control type. For a case of *Transient A*, the constant surface concentration was assumed in which the emission flux varies depending on the ambient concentration distribution of building material (external diffusion control type). For the case of *Transient B*, the emission flux of material surface was set to constant value assuming the inner diffusion control type. The values of constant emission flux and constant surface concentration were established by the fundamental experimental results. The boundary conditions of both transient analyses were assumed, as shown in Table 3-4.

The formaldehyde concentration in water was analyzed by the concentration distribution present in the air. It was assumed that the formaldehyde adsorbed on the water surface; here, the flux conservation was assumed in which the flux that reaches the water surface at the air phase is considered equal to the flux that diffuses into the water. This moves from the air phase to the liquid phase, which requires a unit conversion of concentrations as shown in Chapter 2. Equation (3-3) shows the calculation of concentration in the water using the partition coefficient to consider the change from the gaseous solvent to the liquid solvent.

$$C_w = P_{wa} \cdot C_a \quad (3\text{-}3)$$

Here, C_a and C_w are concentrations in air and water, and P_{wa} is air-water partition coefficient. The P_{wa}, air-water partition coefficient for formaldehyde, which is known as Henry's law constant, was

estimated by the van Hoff equation for considering the test temperature of 20 °C [51, 52]. In addition, water vapor emission form liquid water surface and its diffusion into the air phase were analyses simultaneously, in transient analysis. The transient analyses were carried out over 24 hours as in the formaldehyde emission test.

The initial conditions of formaldehyde and water vapor concentration in the confined desiccator were zero in the transient analysis. The relative residual of the scalar transport equation under transient analysis was confirmed to be reasonably small compared with the threshold value of 10^{-10}, and the time step size (*dt*) of the transient simulation was also carefully set to satisfy the diffusion number.

3.3. Results of numerical analyses

This section presents the results of numerical analyses: *Steady-state*, *Transient A*, and *Transient B*. The transient analysis results show the flux and concentration distribution over 24 hours.

3.3.1. Equivalent diffusion length for different desiccators (Steady-state)

The average one-dimensional diffusion length from building material surface to the water surface, L_d, was calculated using equation (3-2) based on the adsorption flux on the water surface of the steady-state analysis result for the five types of desiccators. Table 3-5 shows the calculation results for steady-state analyses. The calculated L_d values were different for each desiccator. The difference between Type B and Type C was approximately 33%, that of maximum and minimum values. Regarding the influence of the desiccator geometry, the vertical distance from the water surface to the bottom of the building material ($h_{s\text{-}w}$) was varied due to the location of the material and Petri dish. L_d values tend to be proportional to $h_{s\text{-}w}$ values for five types of desiccators, i.e., the L_d is a representative parameter concerning the diffusion formation difference in the confined desiccator. Therefore, the L_d parameters can be used to interpolate the measured emission flux, $flux_m$, for the different geometries of desiccators under the boundary condition of external (evaporative) diffusion control type.

Table 3-5. Calculation results for steady-state analyses

Desiccator	Type R		Type A		Type B		Type C		Type D	
	R-1	R-2	A-1	A-2	B-1	R-1	R-2	A-1	A-2	B-1
Absorption flux, $flux_m$ [$\times 10^{-5}$ μg $m^{-2}s$]	1.92	2.06	1.59	1.62	1.56	1.55	2.33	2.33	1.65	1.66
Equivalent diffusion length, L_d [mm]	852	794	1029	1009	1053	1058	703	703	996	989
Diffusion time scale, τ_d [s]	53 371	46 320	77 838	74 875	81 525	82 353	36 306	36 321	72 878	71 908

The time scale of formaldehyde diffusion in the confined desiccator, τ_d, defined by the diffusion coefficient and equivalent diffusion length was calculated using equation (3-3) (Table 3-5). The τ_d values for all desiccators indicated from 10 to 23 hours, and it was confirmed as not short enough in comparison with the test time of 24 hours.

$$\tau_d = \frac{L_d}{D_a} \tag{3-4}$$

3.3.2. Transient analysis for building material of external diffusion control type (Transient A)

Transient A analysis was performed to confirm the transient nature of the concentration distribution of formaldehyde formation in the confined desiccator (both air and water phase) as a function of time, under the boundary condition of external diffusion control type. Figure 3-3 shows the time series of the averaged emission flux ($flux_m$) on the building materials. The boundary condition of the formaldehyde emission surface was given as the fixed concentration; therefore, the $flux_m$ might have been affected by the formaldehyde ambient concentration of building material, especially just after the start of the test. The time-dependent $flux_m$ characteristics of the material in five desiccators were reasonably consistent with each other, and the equilibrium state was reached within a short time.

Figure 3-4 shows the time series of the adsorption flux on the water surface ($flux_s$). The diffusion time scale was confirmed to be influenced by the desiccator geometry under fixed emission concentration conditions by the steady-state analysis. Therefore, the $flux_s$ was also affected by the desiccator geometry and had a distinct difference for each type.

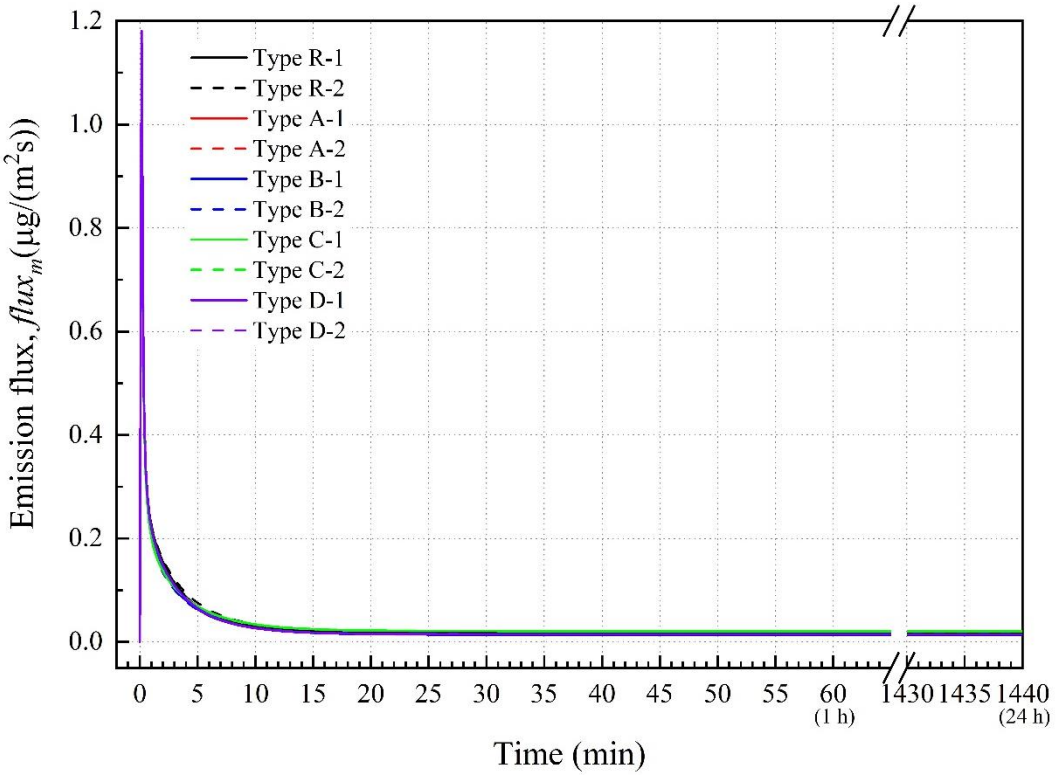

Figure 3-3. Formaldehyde emission flux from the surface of the building materials ($flux_m$) in five types of desiccators in case of the external diffusion control type

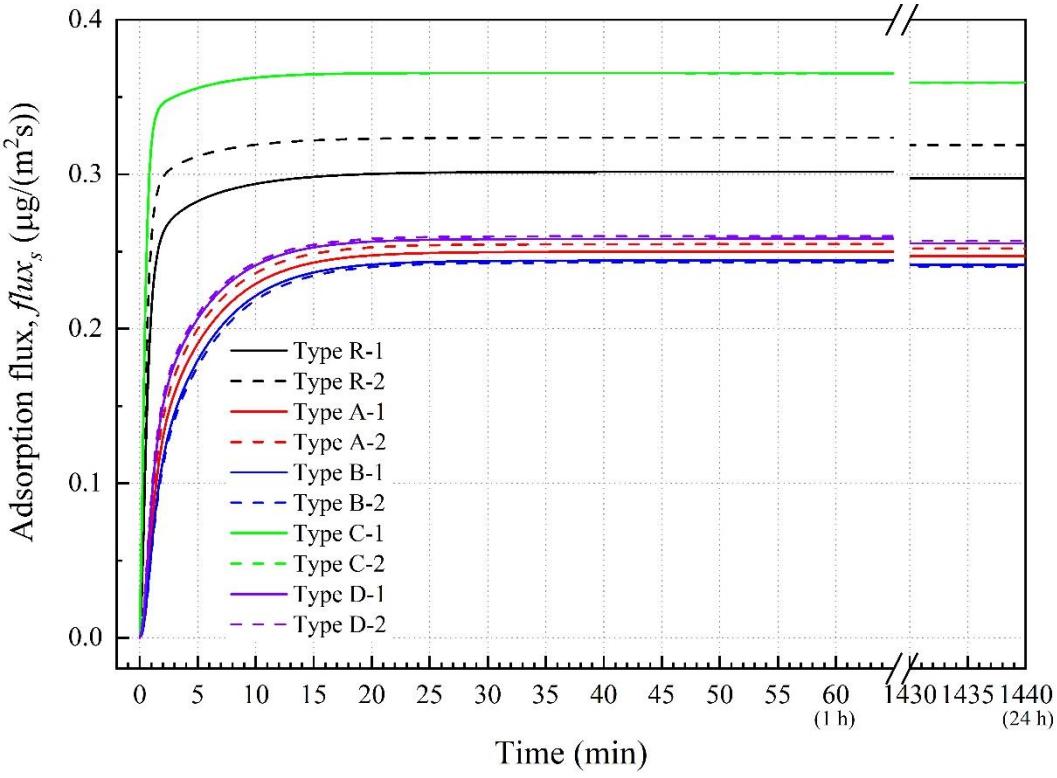

Figure 3-4. Formaldehyde adsorption flux on the water surface ($flux_s$) in five types of desiccators in case of the external diffusion control type

Figure 3-5 shows the time series of the averaged concentration of formaldehyde in water (C_w). The volume-averaged C_w for Type A, B, and D decreased by 19, 22, 17 %, respectively, and that of Type C increased by 17%, compared with that of Type R. These differences were similar to those seen in the L_d value differences, and it indicated the significance of the impact of the desiccator geometry. Also, the volume-averaged C_w was linear during 24 h test time but did not reach the concentration in an equilibrium state (C_{eq}) by the end of the experimental period. Theoretically, the balance between the volume-averaged formaldehyde concentration in both phases (air and water) was expected to be above 2400 h. As shown in Figure 3-4, $flux_s$ on the water surface maintained a maximum level, which was close to the perfect sink condition; that is, there was no transient effect on formaldehyde absorption during the 24 h test time. The formaldehyde emission tests were confirmed reproducible and stable during the test period.

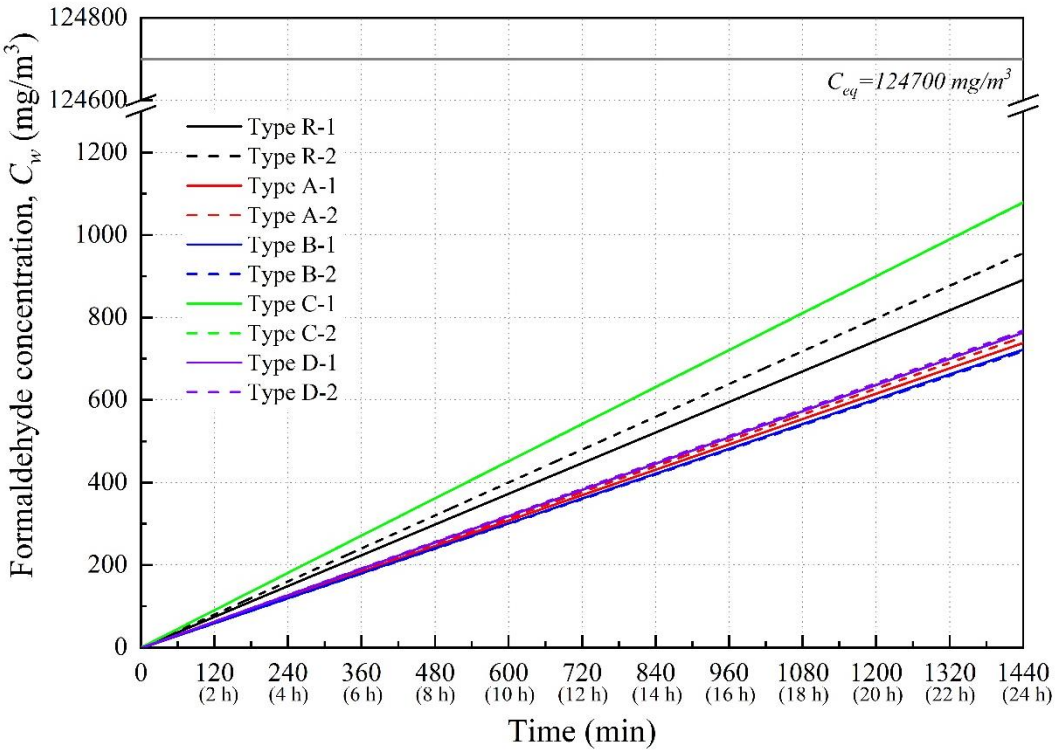

Figure 3-5. Time-series of volume-averaged formaldehyde concentration in the water (C_w) for five different desiccators in case of the external diffusion control type material

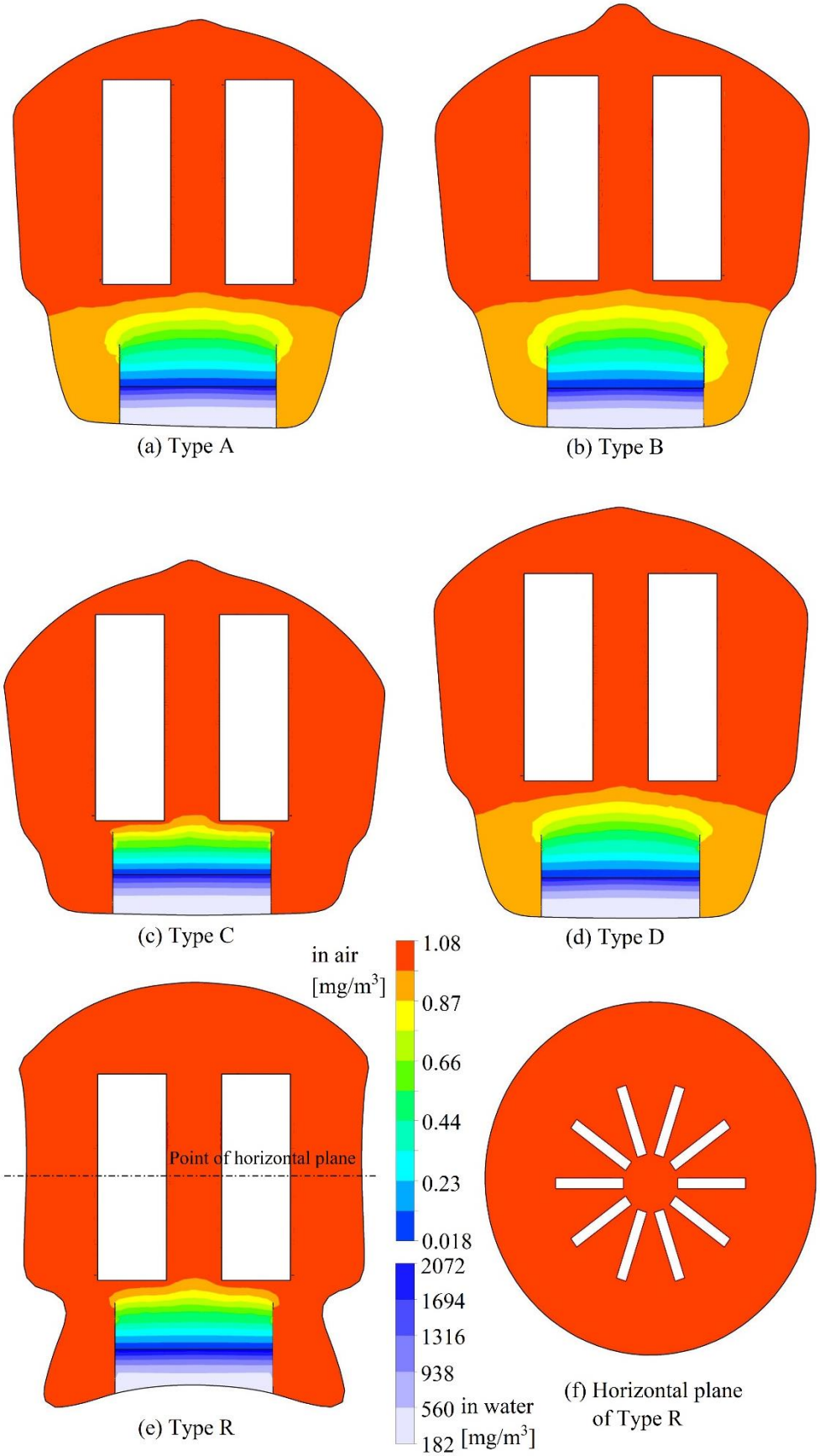

Figure 3-6. Formaldehyde concentration distribution in the air and water measured 24 h after the test start through *Transient A*: (a)-(e) Vertical plane of each desiccator, and (f) Horizontal plane in case of Type R

Figure 3-6 shows the formaldehyde concentration distribution in the air and water for Type R after 24 h. The formaldehyde indicated non-uniform concentration distribution, and it was gradually stratified from the building materials surface to the water surface. The formaldehyde concentration in the air phase had reached an equilibrium. Whereas the formaldehyde concentration distribution in the water phase was confirmed to be gradually linearly stratified from the water surface to the bottom of the Petri dish because the equilibrium has not yet been reached in the water.

The positions of both the test specimen and the sorbent depend on the geometry of the desiccator type; therefore, the vertical distance ($h_{s\text{-}w}$) varied depending on the target desiccator. Figure 3-7 shows the correlation between the L_d value and the volume-averaged concentration of formaldehyde in water depending on the $h_{s\text{-}w}$. The volume-averaged concentration of formaldehyde in the water (C_w) had a negative association with L_d. The L_d values tended to be proportional to $h_{s\text{-}w}$ through *Steady-state* analysis; therefore, C_w was inversely proportional to $h_{s\text{-}w}$. On this basis, it was confirmed that adjusting the $h_{s\text{-}w}$ facilitated consistent results for the formaldehyde emission test regardless of the desiccator type.

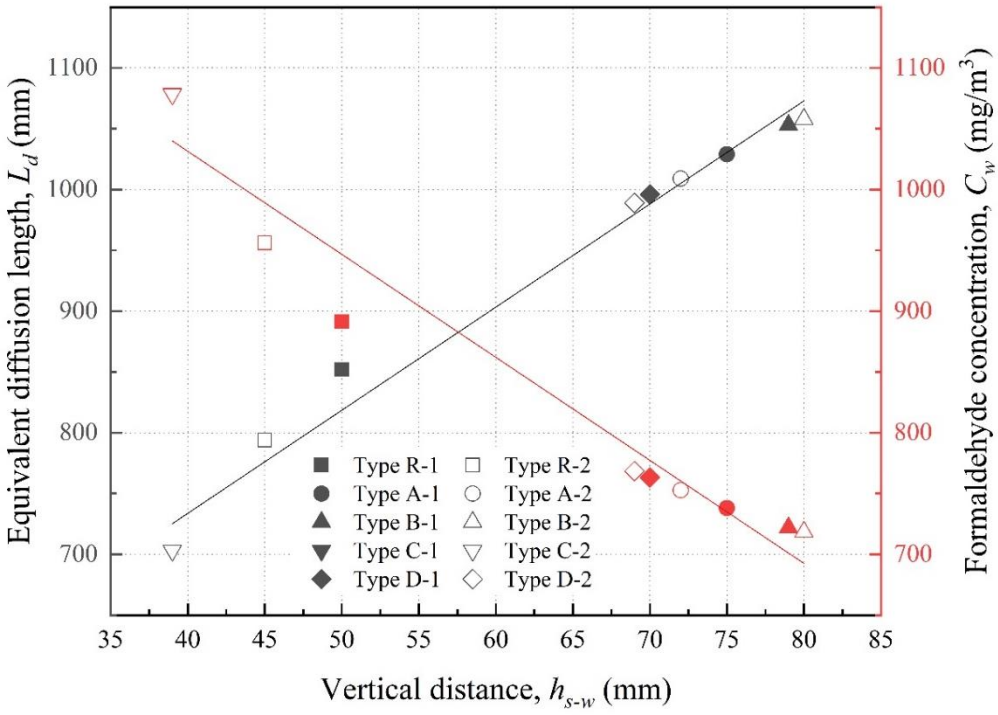

Figure 3-7. L_d value and C_w to the installation location for emission sources for building materials of external diffusion emission control type

3.3.3. Transient analysis for building material of inner diffusion control type (Transient B)

The *transient B* analyses were conducted to confirm the transient of the concentration distribution of formaldehyde formation in five different desiccators when used the building materials of the inner diffusion control type.

Figure 3-8 shows the time-series of the formaldehyde adsorption flux on the water surface ($flux_s$). The boundary condition of the formaldehyde emission surface was given a fixed flux to reproduce the inner diffusion control type emission characteristics in two cases of the high- and low- emission rates. These boundary conditions were not affected by the formaldehyde concentration distribution in the air. Whereas in the boundary condition of the adsorption surface, the flux was preserved on the sides of the air and water and influenced by the ambient concentration on the water surface on both sides. The time required to reach a quasi-steady state and the adsorption flux on the water surface differed between the detector type until reaching an equilibrium state; however, all cases attained a quasi-steady-state condition in terms of $flux_s$ on the water within 8 h, which may be a short time scale compared with the total experimental duration of 24 h. The time-dependent $flux_s$ characteristics for the desiccator types were reasonably consistent. Therefore, it is confirmed that estimated adsorption flux is hardly affected by desiccator geometry when used the inner diffusion control type material. Figure 3-9 shows the time-series of the average concentration of formaldehyde in the water (C_w) for five different desiccators using the high- and low-emissions material. The volume-averaged C_w continued to increase in all desiccators through the end of the 24 h test duration. The adsorption on the water surface and the increase in volume-averaged C_w continued to occur even though the formaldehyde concentration in the air reached the equilibrium state because of the sizeable air-water partition coefficients of formaldehyde. The differences of estimated volume-averaged C_w for each desiccator after the end of 24 h test time was not significant. That is, assuming the building material of inner diffusion control type, there is a time difference in which the average concentration in the air reaches a steady-state, but since the same amount of emission is emitted regardless of the desiccator geometry, the measurement results for the test time (24 h) are virtually the same.

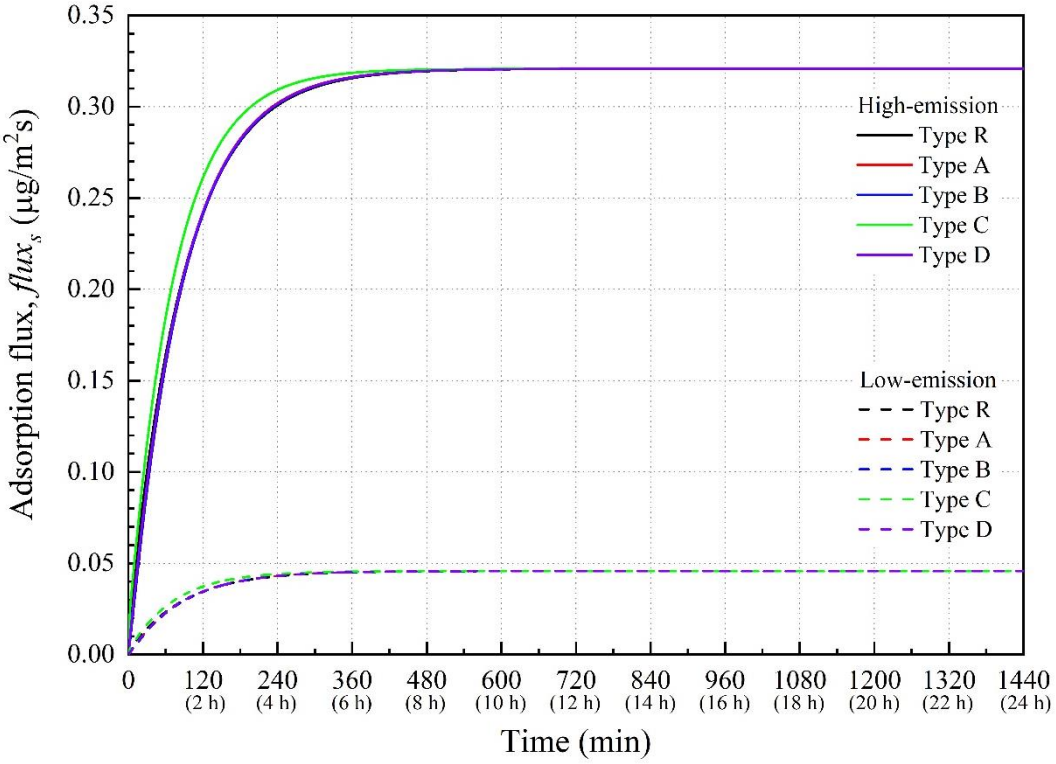

Figure 3-8. Formaldehyde adsorption flux on the water surface ($flux_s$) in five types of desiccators in case of the inner diffusion control type material

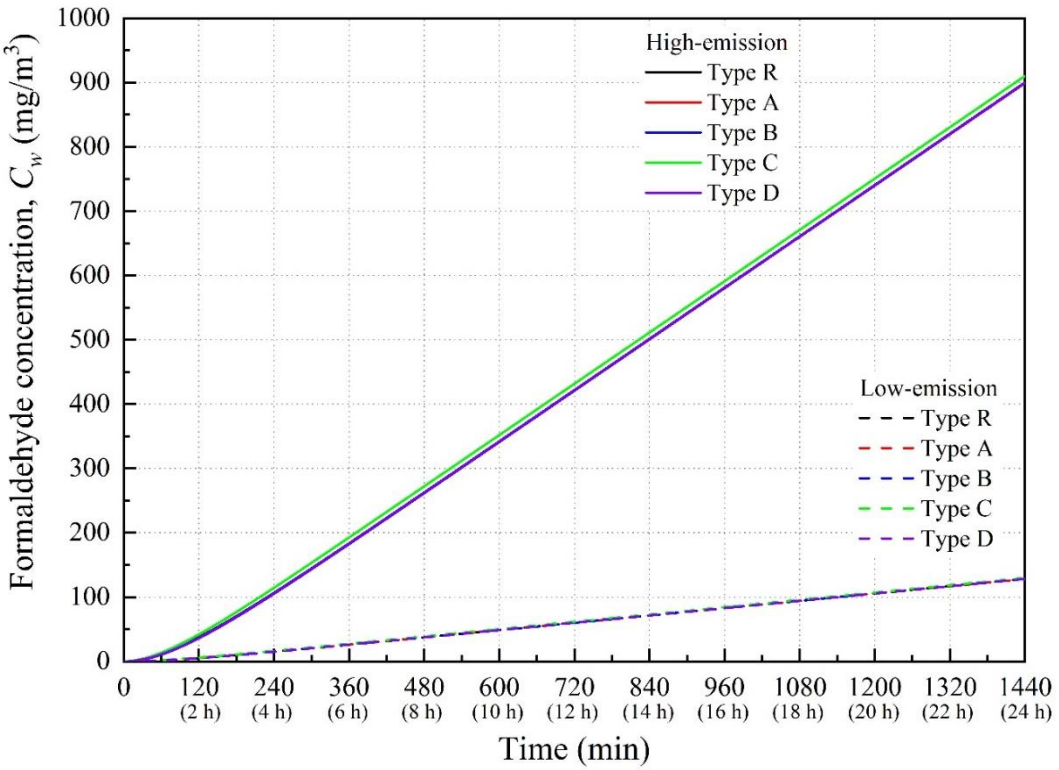

Figure 3-9. Time-series of volume-averaged formaldehyde concentration in the water (C_w) for five different desiccators in case of the inner diffusion control type material

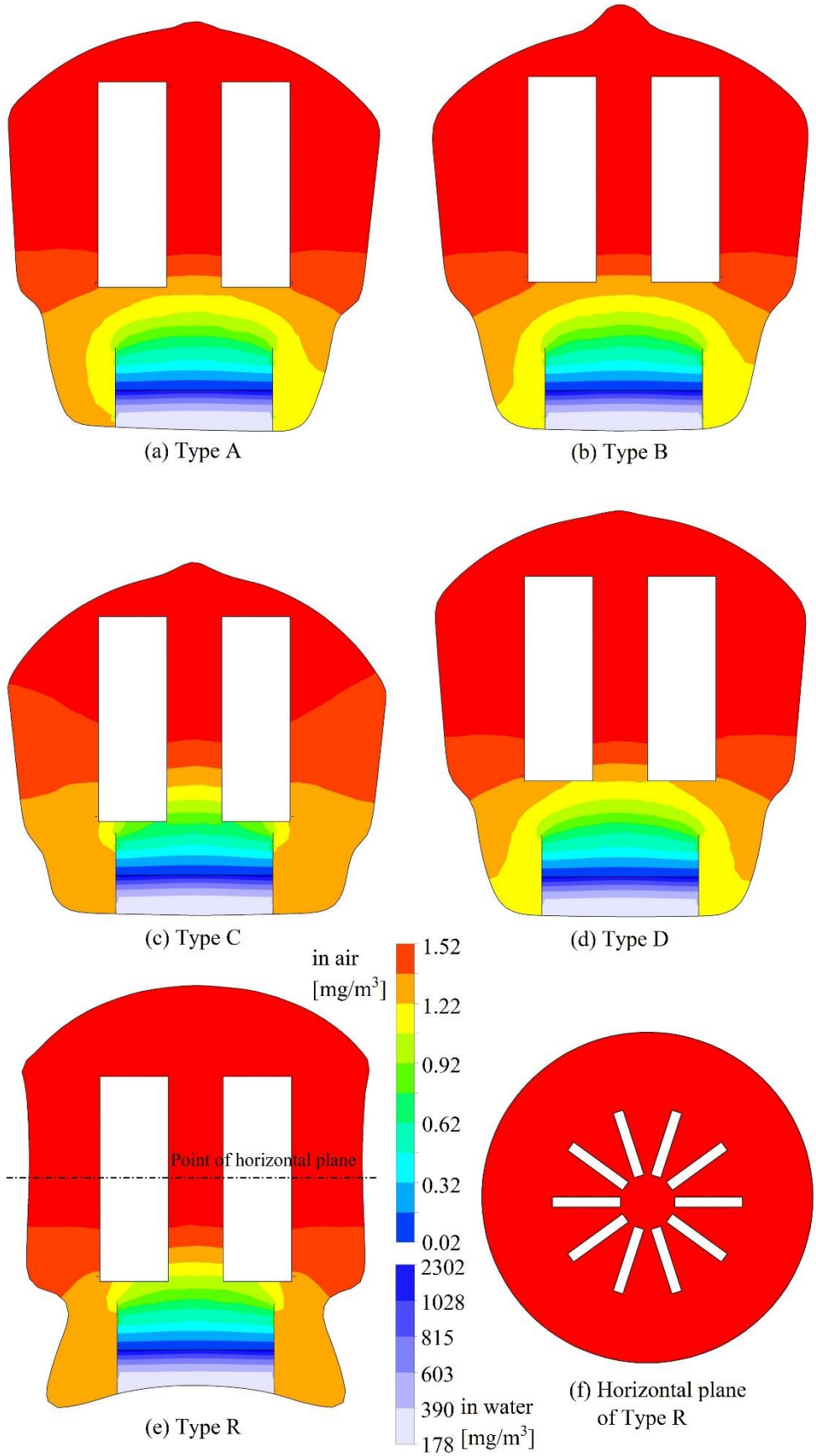

Figure 3-10. Formaldehyde concentration distribution in the air and water measured 24 h after the test start through *Transient B* with the high-emission materials: (a)-(e) Vertical plane of each desiccator, and (f) Horizontal plane in case of Type R

Figure 3-10 shows the formaldehyde concentration distributions in five different desiccators after the 24 h test period. The concentration distribution formation in the vicinity of building materials was indicated different, however, it showed a non-uniform concentration distribution in the desiccator which was similar to the results of *Transient A* (Figure 3-6).

3.4 Discussion

This section presents the effect of moisture on the formaldehyde diffusion and the additional analysis of the correlation method for changes in the diffusion field.

3.4.1 The change of diffusion coefficient in a three-component gas mixture

The diffusion coefficient of formaldehyde in the gas phase is the dominant factor with respect to its emission and absorption to the water in the desiccator. In accordance with JIS standard, formaldehyde emission testing was conducted under an isothermal condition 20 °C, with no humidity requirement prescribed. In confined desiccator environment, water installed as a sorbent evaporates, and will gradually distribute itself as heterogeneous humidity inside the desiccator, before eventually reaching equilibrium, becoming distribution uniformly at saturated vapor pressure. It suggests that the water vapor concentration might affect the formaldehyde diffusion coefficient in the gas phase in the desiccator. Therefore, this study evaluated the change of formaldehyde diffusion coefficient by moisture behavior in the confined desiccator, using the transient analysis considering the three-component gas mixture consisting of formaldehyde, water vapor, and dry air.

Figure 3-11 shows the time-series of the water vapor flux on the water surface and the volume-averaged concentration of water vapor in the confined desiccator. The initial relative humidity in the desiccator was set as zero, i.e., the perfectly dry condition, and it was indicated that water vapor in the desiccator became saturated within 4 h of the test start. The formaldehyde diffusion coefficient value from the two-component system to the three-component system changed slightly from 0.136 to 0.137 cm^2/s; that is, the change was within 1%. It was determined that the impact of transient humidity

change in the air was almost negligible, for the 24 h test period.

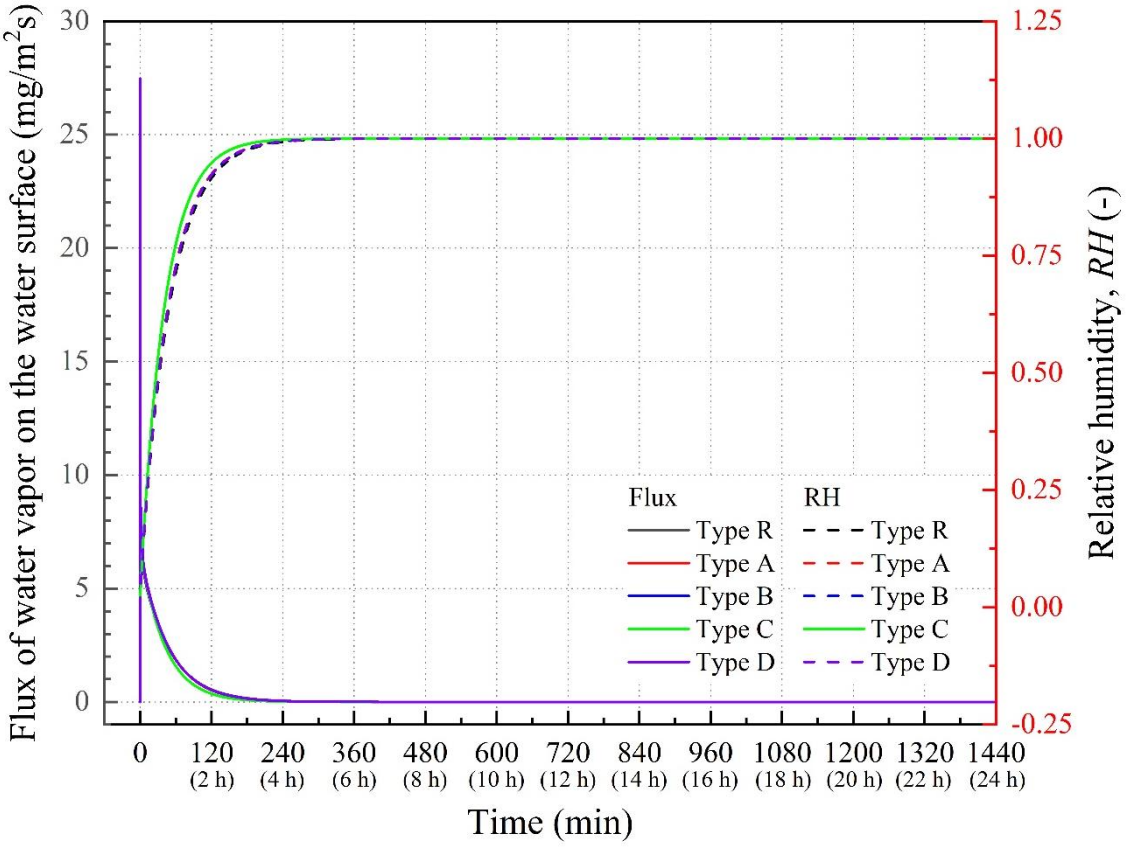

Figure 3-11. Time-series of water vapor flux on the water surface and volume-averaged water vapor concentration in the desiccator for 24 h test time

3.4.2 Sensitivity evaluation of L_d value

The L_d is a sensitive parameter related to all installed components in the diffusion field. To clarify the sensitivity of L_d, a steady-state analysis was performed using the desiccator model excluding the edge of the crystal dish as shown in Figure 3-12. As the results of the steady-state analysis, L_d values were shown to have decreased by approximately 60% to 523, 648, 672, 432, and 622 mm in each type of desiccator. Figure 3-13 shows the distinct differences in the formaldehyde concentration distribution over the adsorption surface compared with the results of the previous model. The L_d is a representative parameter that quantitatively investigates the differences in the desiccator geometry. However, it is also a sensitive parameter that is influenced by the detailed conditions of the research environment.

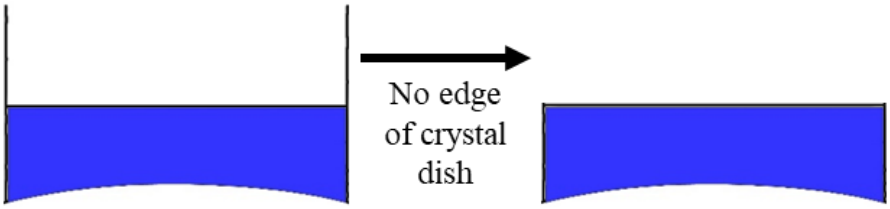

Figure 3-12. Installation model without accounting for the edge of the crystal dish

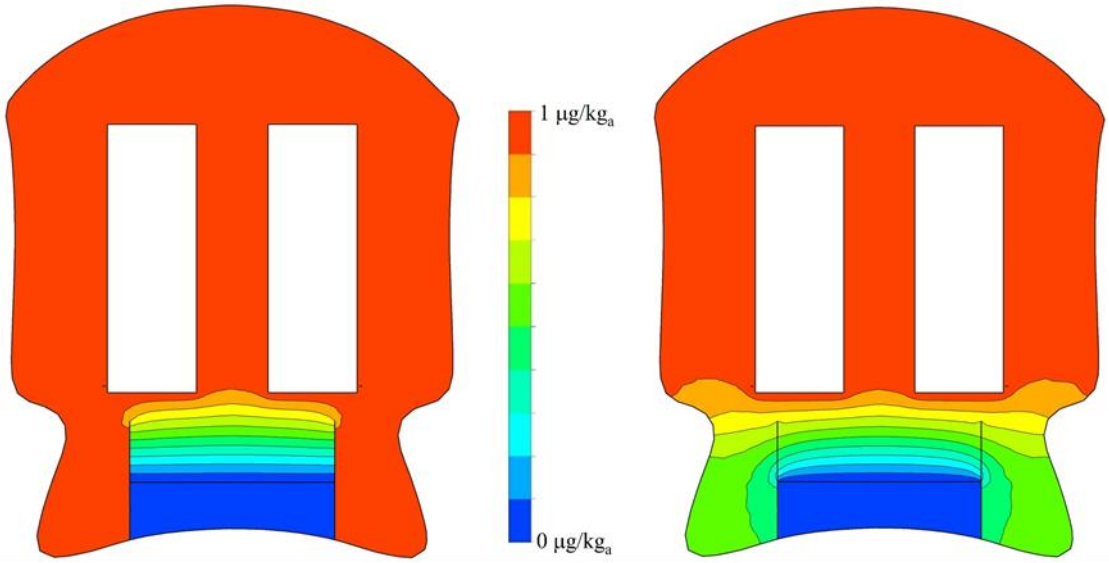

Figure 3-13. Result of the formaldehyde concentration distribution in a modified model without considering for the edge of the crystal dish (Type R): (a) previous model, and (b) modified model

3.4.3. Correlation between L_d and emissions results

According to analyses of *Steady-state* and *Transient A*, the L_d was a representative parameter for changes in formaldehyde emission flux according to geometrical differences of the desiccators. It is expected that formaldehyde emission rates will be calculated identically despite the desiccator geometrical differences when L_d is adjusted equally. The three models were therefore prepared with the same L_d value by modifying the vertical distance from the bottom of building material to the water surface using the four desiccators of Type R and Type A. The desiccator models modified to equal the L_d value of Type R-2 which is 794 mm, as shown in Figure 3-14.

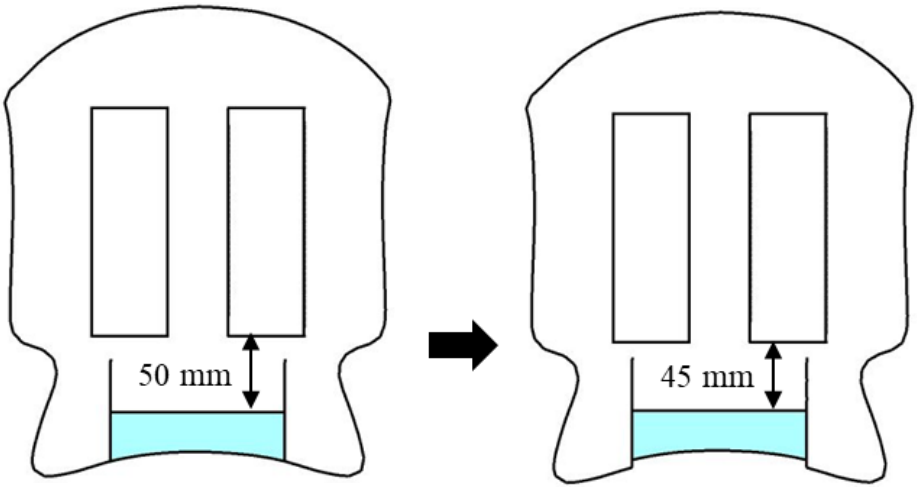

Figure 3-14. A modified model for Type R-1 with $h_{s\text{-}w}$ length adjusted (the L_d value is 794 mm)

Transient analyses were conducted assuming the different boundary conditions on the emission surface for both cases of the external and inner diffusion control type. In the case of the inner diffusion control type material, the analysis was performed to high emission rates. Figure 3-15 shows the time-series of the volume-averaged concentration of formaldehyde in the water (C_w) for four desiccator models. For external diffusion control type, noticeable changes occurred owing to the modification of L_d, as shown in Figure 3-15(a). The volume-averaged C_w was different among the four types of desiccators prior to L_d value correction, although the concentration was similar to the Type R-2 after modification. The diffusion resistance in the air, up to the absorbent surface of the water from the material emission sources, controlled the total amount of formaldehyde emitted from the building material. However, in models of the inner diffusion control type, the change in volume-averaged C_w was insignificant, and its difference in the C_w value after the 24 h testing was less than 1%, as shown in Figure 3-15(b). That is, the results for the formaldehyde emission rates showed almost no difference from the results of *Transient B* (Figure 3-9). Therefore, it was confirmed that the formaldehyde emission rates are not substantially affected by the L_d value and the desiccator geometry when the flux of the emission surface is constant.

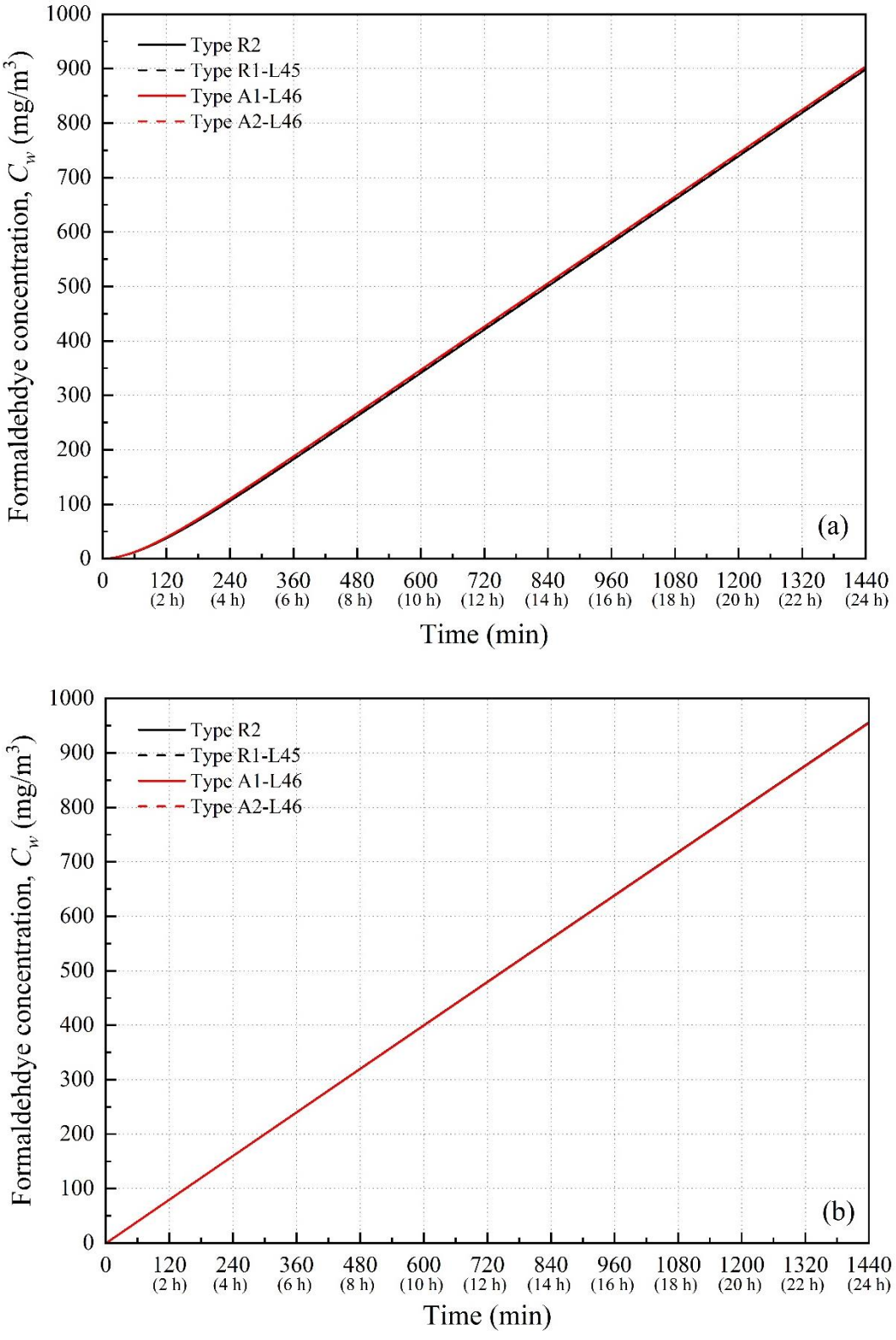

Figure 3-15. Time-series of volume-averaged concentration of formaldehyde in water (C_w): (a) external diffusion control type, and (b) inner diffusion control type

The results of the *Steady-state* and *Transient A* analyses, which considered the formaldehyde adsorption and diffusion in the water, confirmed that the formaldehyde emission rate is controlled by L_d when modeled by using external diffusion control materials. On this basis, it is emphasized that the time series of the formaldehyde emission and adsorption ($flux_m$ and $flux_s$) immediately after the test start depend strongly on the desiccator geometry and the relative positional relationship between the building material and water surface. Therefore, for the external diffusion control type, in which formaldehyde emission from building materials is assumed to have a constant surface concentration, this analysis demonstrates the dependence of the emission rate on the desiccator geometry and proposed the concept of L_d to calibrate the measurement results.

The building materials can be categorized into two groups the point of formaldehyde emission: inner diffusion control type and external diffusion control type. Whereas some building materials might indicate the intermediate characteristics between inner diffusion and external diffusion, and these emission characteristics can be approximately described and formulated the combination of both diffusion mechanisms. This simplified modeling might be the linear coupling of inner diffusion and external diffusion mechanisms. Provide that the adsorption onto the inner wall surface of desiccators and chemical reactions are disregarded, formaldehyde emission diffusion in air and dissolution (adsorption) into the water can be formulated as the linear system, as shown in the governing equation of this study (equation (3-1)). It was supposed that the simplified inner diffusion type and external diffusion type can cover the majority of general building materials.

3.5. Limitations of this study

In numerical analyses, it was assumed to the isothermal condition that the possibility of temperature change due to water evaporation such as latent heat was disregarded. Further, the potential impacts of radiative heat transfer onto the glass or water surface were assumed to negligible and were discounted. The buoyancy effects caused by temperature and humidity differences were confirmed to be negligible, therefore, its effects were not applied to the analytical model [53].

The adsorption of formaldehyde in the borosilicate glass, the principal material of the targeted desiccators, is smaller than the adsorption or trapping to the water. The time for the formaldehyde concentration in air in the desiccator to reach a steady-state was estimated shorter than the test time of 24 hours. Therefore, the effect of adsorption on the glass surface of desiccator on the formaldehyde concentration distribution is considered insignificant.

For the numerical analyses, securing quality control such as a grid independence check was carefully conducted. The time step size for the transient analysis was determined to satisfy the Courant–Friedrichs–Lewy condition and very strict convergence criteria (order of residual < 10^{-10}) was adopted. The numerical analyses were conducted under simplified boundary conditions and were confirmed to provide a sufficient guaranteed prediction accuracy. However, this study only used results from the numerical method and did not include any experimental results. The numerical simulation results should be validated by experimental results. Thus, highly accurate experimental data would be needed for the verification of the numerical analysis. This is to be conducted in our future work. Furthermore, verification of the prediction accuracy of numerical analysis with experiments, for the external diffusion control type building material should be performed in future work.

3.6 Conclusion

In this chapter, the transport of moisture and chemicals due to molecular diffusion in a confined analysis environment system is analyzed. Especially, the numerical analyses were conducted on the diffusion properties of chemicals.

In terms of chemical emission conditions, the diffusion of chemicals is affected by the shape of diffusion field; especially in the case of external/evaporative diffusion control type that assumes the emission concentration from building material is fixed, the resultant value for the measurement time differs depending on the desiccator geometry. In other words, in the environment considering only molecular diffusion, it was confirmed that the diffuson phenomenon of chemicals varies depending on the shape of the diffusion field so that sufficient consideration is needed when reproducing the diffusion field geometries.

Furthermore, by analyzing the results of the transient analysis using a model that reproduces water vapor generation and diffusion phenomena, it was found that the diffusion coefficient of chemical is changed due to moisture.

Although analyzing chemical transport was possible in a simple and quick time using a confined desiccator, only molecular diffusion without airflow under isothermal conditions is calculated. In this regard, the next chapter introduces the development of a model for the advection-diffusion environment system in the indoor that reproduces fluid flow, temperature and humidity changes, and chemical diffusion.

CHAPTER 4

Hygrothermal – Chemical Transport in a Room with 3D Digital Clothed Model integrated with Computer-Simulated Person

4.1 Foreword

Numerical analysis using a confined desiccator is performed under restricted conditions in Chapter 3, which is a simple method of determining the concentration distribution of chemicals in space in terms of its molecular diffusion. However, the results of this numerical analysis are different from results for hygrothermal and chemical transport phenomena in an indoor environment considering heat transfer and turbulence diffusion.

Against this background, this chapter describes developing a model to analyze detail regarding the transport of heat, moisture, and chemicals by reproducing the indoor environment system. At this time, a CSP model applicable to CFD simulation was used to predict the influence of the human body located indoors.

In terms of the CSP model, the computational human model integrated with the thermoregulation model that has been suggested to predict skin surface temperature distribution and thermal comfort of the human body is used in research related to indoor thermal environmental analysis. However, clothing has been treated with simplification as a resistance of hygrothermal transfer, and airflow and hygrothermal transfer phenomena in and around clothing with the complex geometry of clothes have not been fully discussed. Therefore, this chapter applied the CSP integrated with the clothing model that reproduced the complex clothing shape to the numerical analysis model for indoor environment system developed in this chapter, and analyzed hygrothermal and chemical transports in the human-indoor environment system. In this study, the target chemical is formaldehyde.

4.2 Methodology

4.2.1 3D modeling

To develop a CSP including the complex geometry of clothing appliable to CFD simulation, thermal manikin, and clothes (T-shirt and pants) were prepared. A three-dimensional (3D) digital model with detailed geometry of manikin and clothes was generated using a laser 3D scanner (EXAscan, CREAFORM), as shown in Figure 4-1. The precision of the scan data was approximately ± 0.055 mm. To obtain the detailed geometric structure of the air layer between the skin and clothes, the manikin and clothes were scanned individually, and their geometric data were rearranged appropriately to create an analytical mesh inside the air gap. In this section, a short-sleeved T-shirt and pants were prepared as representative types of clothing. The area inside clothing with 1 mm thickness was reproduced to investigate the transport of thermal, humidity, and contaminants in clothes.

(a) (b)

Figure 4-1. Three-dimensional (3D) digital model of thermal manikin and clothes: (a) Manikin and (b) T-shirt and Pants

4.2.2 Outline of the numerical analysis

The object of the CFD simulation is a rectangular room in which the developed CSP at the center. The outline of the analytical domain and grid design is shown in Figure 4-2. A CSP was located at the center of the simple room model of 3 × 3 × 3 m. The model has a supply inlet with dimensions of 1 × 0.3 m at the lower part of the front wall and an outlet with dimensions of 1 × 0.3 m at the upper part of the back wall. The analytical domain was discretized with polyhedral meshes, and three prism mesh layers were created in the vicinity of the skin, clothes, and wall. To reproduce the complex geometry of the clothes and the narrow space between the clothes and skin, the surface meshes in that region were arranged denser.

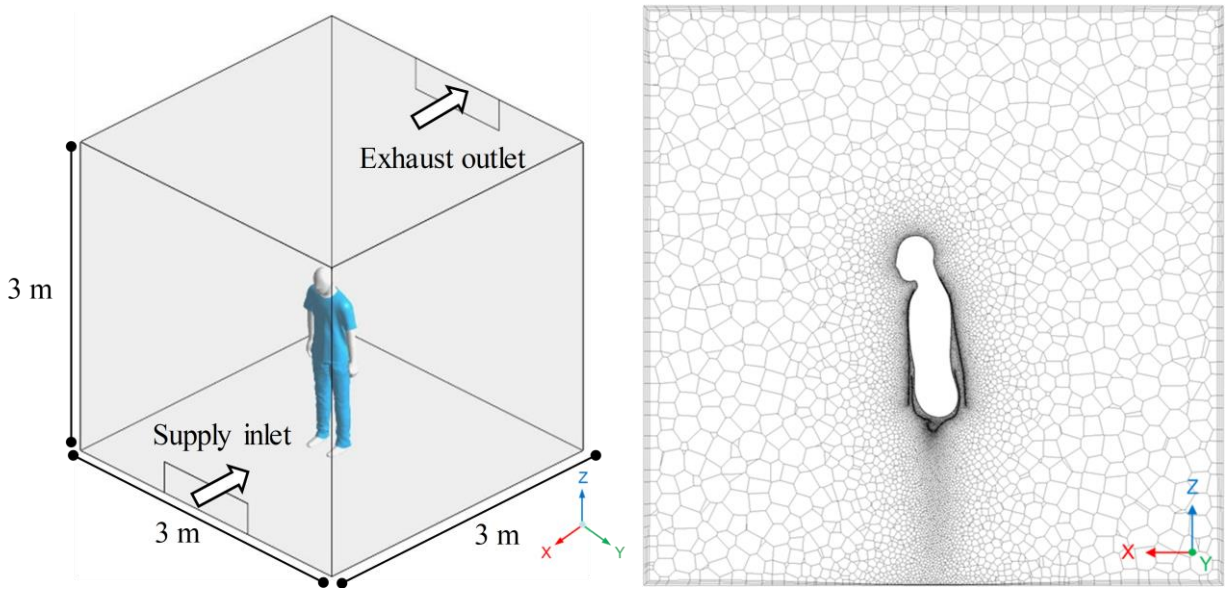

(a) (b)

Figure 4-2. Outline of the analytical domain and grid design around CSP with the clothing model: (a) Outline and (b) Grid design

To clarify the change in exposure concentration of the human body according to the presence or absence of clothes, cases of naked and clothed models, Case-N and Case-CL, respectively, were prepared. In addition, a case study, as summarized in Table 4-1, under various thermal conditions and the emission location of formaldehyde, was performed to confirm the impact of temperature, humidity,

and contaminant distribution characteristics on hygrothermal and multi-component chemical transport. The analytical and boundary conditions for the CFD simulation are given in Table 4-2.

Table 4-1. List of analytical cases

Case	Clothing condition	Emission location of formaldehyde	Thermal condition of supply air
Case-N1	Naked	Wall surface in front of CSP	T_{in} = 300 K, X_{in} = 50%RH
Case-N2			T_{in} = 288 K, X_{in} = 50%RH
Case-CL1	Clothed (T-shirt and pants)		T_{in} = 300 K, X_{in} = 50%RH
Case-CL2			T_{in} = 288 K, X_{in} = 50%RH
Case-CL3		Floor surface	T_{in} = 300 K, X_{in} = 50%RH
Case-CL4			T_{in} = 288 K, X_{in} = 50%RH

Table 4-2. Analytical and boundary conditions

Turbulence model		Low Re number k-ε model (Abe-Kondoh-Nagano model)
Algorithm		Coupled for pressure-velocity coupling 2nd order upwind scheme for convection
Total number of meshes		Case-N: 1.2 million (Naked model) Case-CL: 4.0 million (Clothed model)
Inflow boundary		Velocity inlet, U_{in} = 1.0 m/s, TI = 10%
Outflow boundary		U_{out}, T_{out}, X_{out} = Gradient zero
Wall treatment	Room	Velocity: no slip Temperature, humidity, and contaminant: Gradient zero
	Human body	Velocity: no slip Temperature: calculated by thermoregulation model (Fanger's 1-node model) Humidity: X_{skin} = 0.01449 kg/kg' (const.) Contaminant: C_{skin} = 0 μg/m^3 (perfect sink)
	Clothing	Velocity: no slip Temperature, humidity, and contaminant: flux conservation (air-cloth partition coefficient: $P_{cloth:air}$ = 4.48 × 10^3
Formaldehyde emission flux (front wall or floor surface)		$Flux$ = 0.345 μg/m^3

Turbulence has been analyzed through the Navier-Stokes and the continuity equation applied Low-Reynolds number type k-ε model (Abe-Kondoh-Nagano model). The CFD simulation coupled with temperature, humidity, and contaminant (here formaldehyde) distribution analysis was conducted. Surface to surface (S2S) model was also used to analyze radiant heat transfer. These numerical conditions have already been explained in Chapter 2.

The inflow velocity was assumed to be 1 m/s so that the formaldehyde concentration in the room can reach a steady-state within a short time. The building material with a fixed generation rate of

formaldehyde was set in the room, assuming an indoor perfect mixing concentration of 10 μg/m^3, which was equivalent to 10% of the guideline value in the World Health Organization (WHO) air quality guidelines [54]. The formaldehyde emitted from the wall or floor surface is adsorbed and desorbed on the clothing surface and is transferred to the skin surface having a relatively low concentration. The flux conservation on the clothing surface for heat, moisture, and contaminants, was considered and calculated. In mass transfer, clothes are assumed to be in a solid phase, and unit conversion for the concentration of contaminants unit is required since the density varies. The air-cloth partition coefficient ($P_{cloth:air}$) for unit conversion was estimated using the experimental results obtained by formaldehyde adsorption of a cotton patch in accordance with a change in formaldehyde concentration in the air using a desiccator [55].

For formaldehyde diffusion in the air, the molecular diffusion coefficient in a three-component gas mixture (contained dry air, moisture, and contaminant) was calculated considering temperature changes. In the clothing, the transfer of heat and moisture was determined by a hygrothermal transfer model described in Chapter 2. In Equations (2-38) and (2-39), the κ value is estimated based on the experimental results of a previous study on the isothermal adsorption of water vapor in cotton fiber [56]. While the formaldehyde diffusion coefficient was updated by temperature and humidity in the local region.

For the quality control of CFD simulation using a CSP, advisable analytical methods suggested in a previous study, including grid design in the analytical domain, were applied in this section [57-64]. The minimum thickness of the boundary mesh, skewness, and size ratio of adjoining mesh in the entire domain was elaborately designed, and grid independence was carefully checked under the considering of the complex features of the clothing model. The anlaysis/boundary conditions in this simulation were also thoroughly established. The total calculation time was 10 min (600 s), and the time step sized (dt) of the transient analysis was carefully set to satify the Courant-Friedrichs-Lewy (CFL) condition [65].

4.3 Results and discussion

This section presents the results of hygrothermal and chemical transports in the room for six cases of different conditions. To clarify the change due to the clothing model, the temperature, humidity, and chemical concentration near the surface of clothing were confirmed at certain points.

4.3.1 Indoor airflow distribution

The indoor airflow distributions in six cases after 10 min of calculation period are demonstrated in Figure 4-3. A non-uniform distribution of scalar velocity was found in the entire space of the room. The airflow was observed to flow toward the exhaust outlet after passed the lower part of the CSP and reached the back wall. It was also shown that the thermal plume around CSP occurred by the buoyancy effect was not clearly confirmed because of the airflow pattern around CSP, which is relatively dynamic. The overall airflow distributions of Case-N1 and Case-N2 were similar. However, insignificant differences were presented between Case-CL1 and Case-CL2, as well as Case-CL3 and Case-CL4. This difference can be attributed to the flow filed in cases with clothing were in the transitional stage under complicated flow patterns resulted from the complex geometry of the clothed model, while a simple flow pattern was formed around the relatively flat geometry of the naked model.

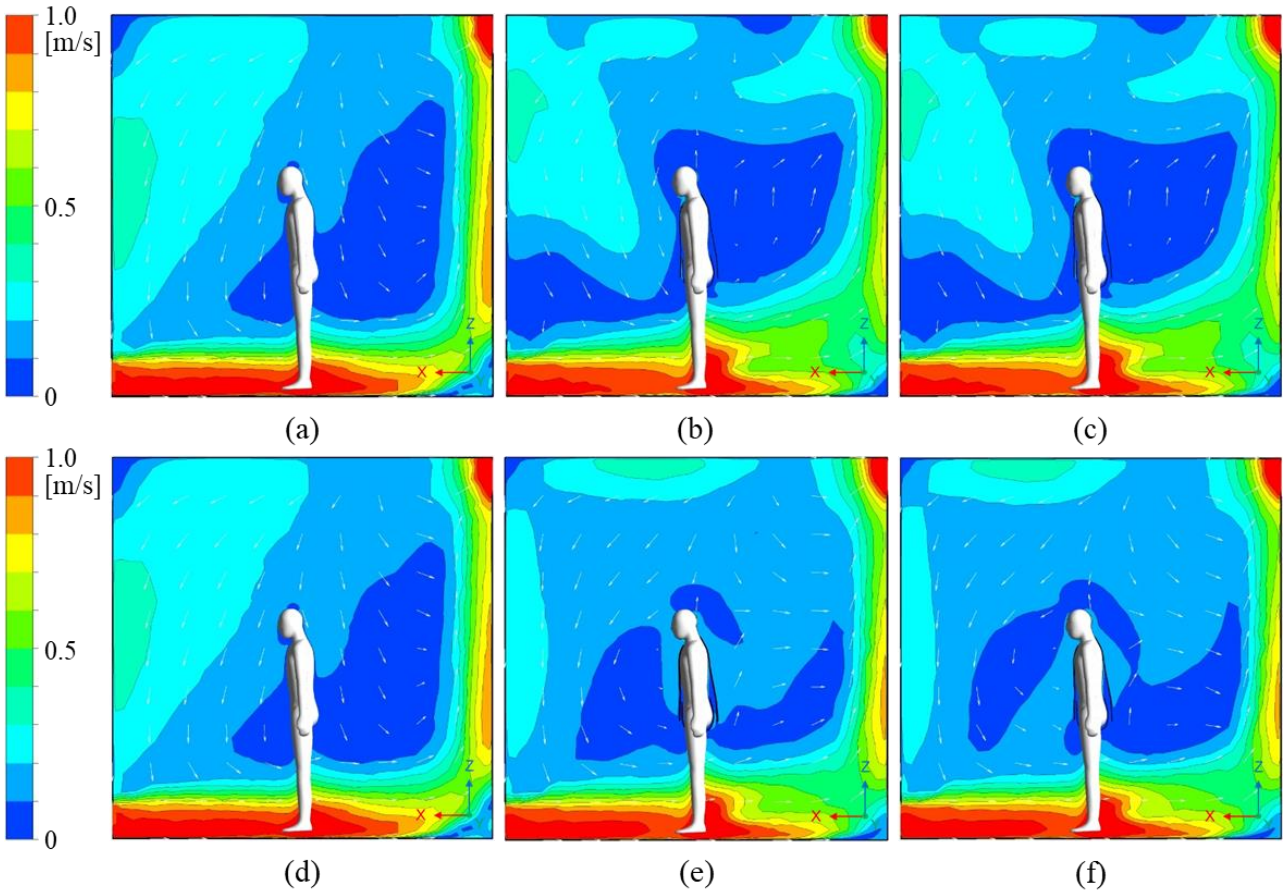

Figure 4-3. Indoor airflow distributions for six cases: (a) Case-N1, (b) Case-CL1, (c) Case-CL3, (d) Case-N2, (e) Case-CL2, and (f) Case-CL4

The local airflow distribution analysis results around clothing for Case-CL1 and Case-CL2 are shown in Figure 4-4. A greater temperature difference between the CSP and surrounding environment leads to an increase in buoyancy intensity; therefore, a stronger ascending air current around clothing was confirmed in Case-CL2. It also means that various thermal environmental conditions may have a certain impact on the ventilation rate inside the air gap.

In addition, both a forced inflow in the high-velocity region and natural inflow resulting from buoyancy inside the air gap was observed. At the exit of the ventilation layer, the ascending air current escaped with a relatively high velocity because of the confined space and narrow escape near the neck part. From this result, satisfactory consistency for the result of the ventilation flow rate inside the air gap was confirmed with previous studies [25, 66].

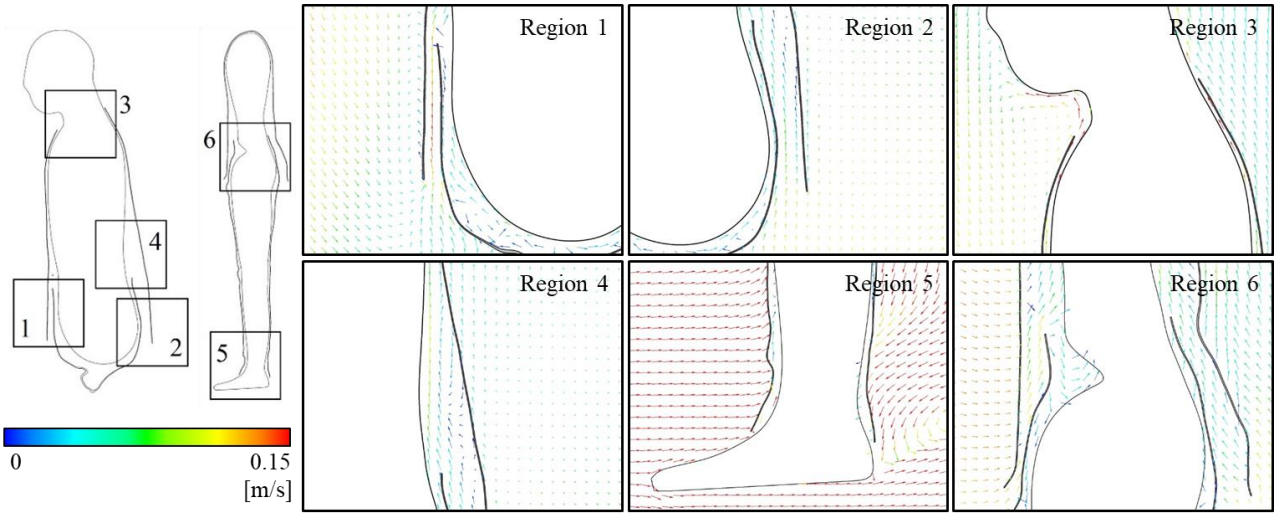

(a)

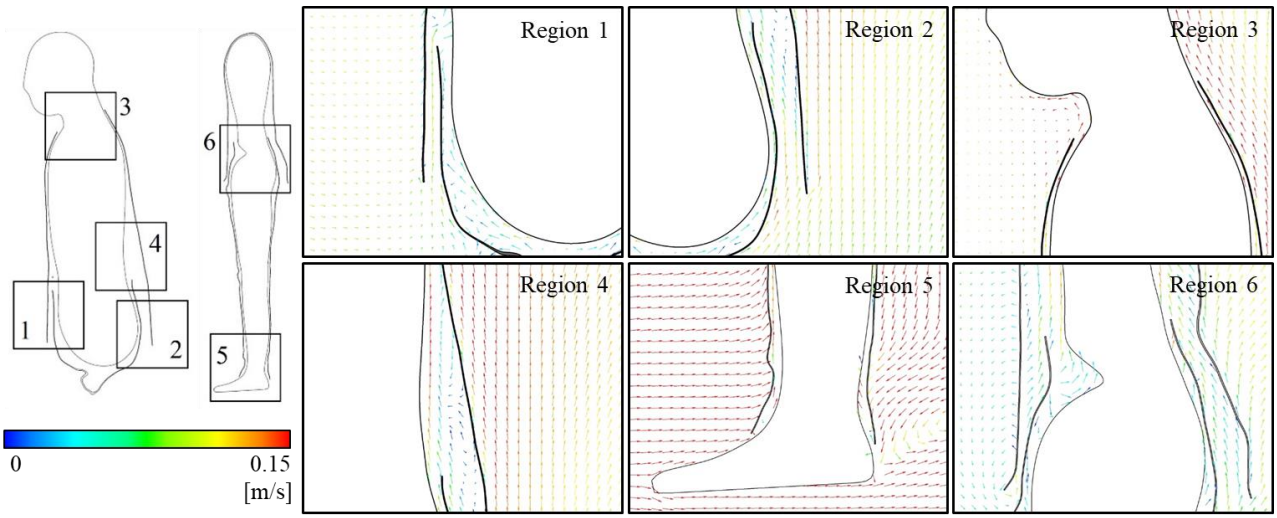

(b)

Figure 4-4. Local airflow distribution around clothing at t = 600 s: (a) Case-CL1 and (b) Case-CL2

4.3.2 Hygrothermal distribution

The temperature and humidity distribution analysis results around CSP were indicated in Figure 4-5. In the uniform distribution of temperature and humidity in the entire indoor space, a higher temperature and humidity distribution was found in the area between clothing and the human skin surface due to heat resistance of clothing that inhibited temperature and humidity diffusion from the human body. The temperature and humidity in the room, which are not shown in the figure, were similar to the set value of the inlet air and the distributions are insignificant.

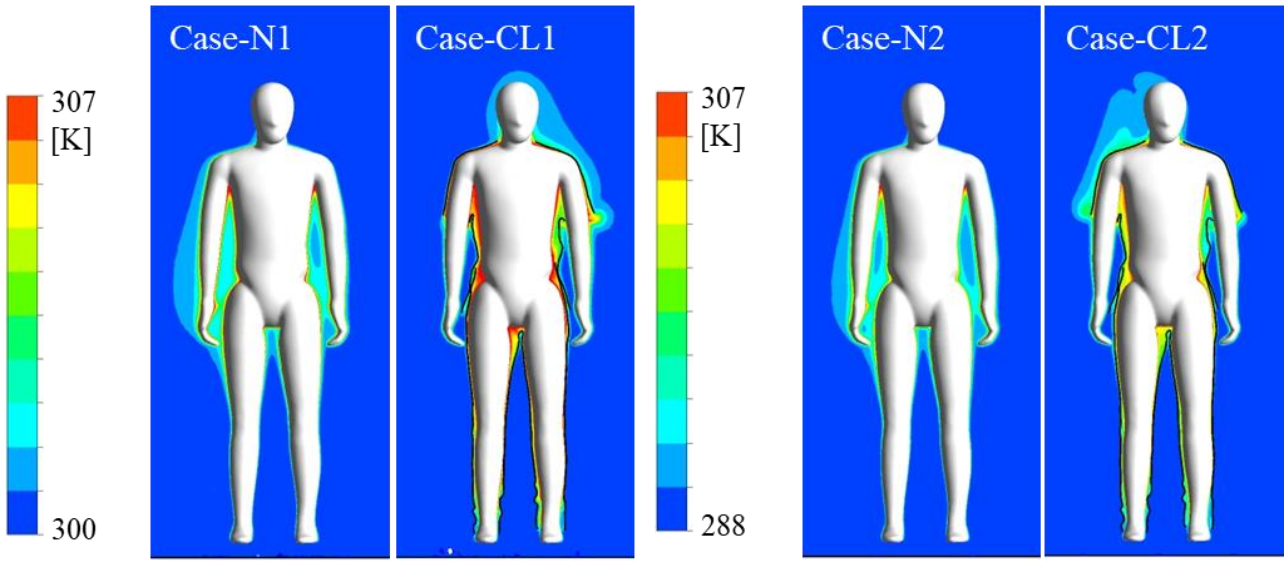

(a)

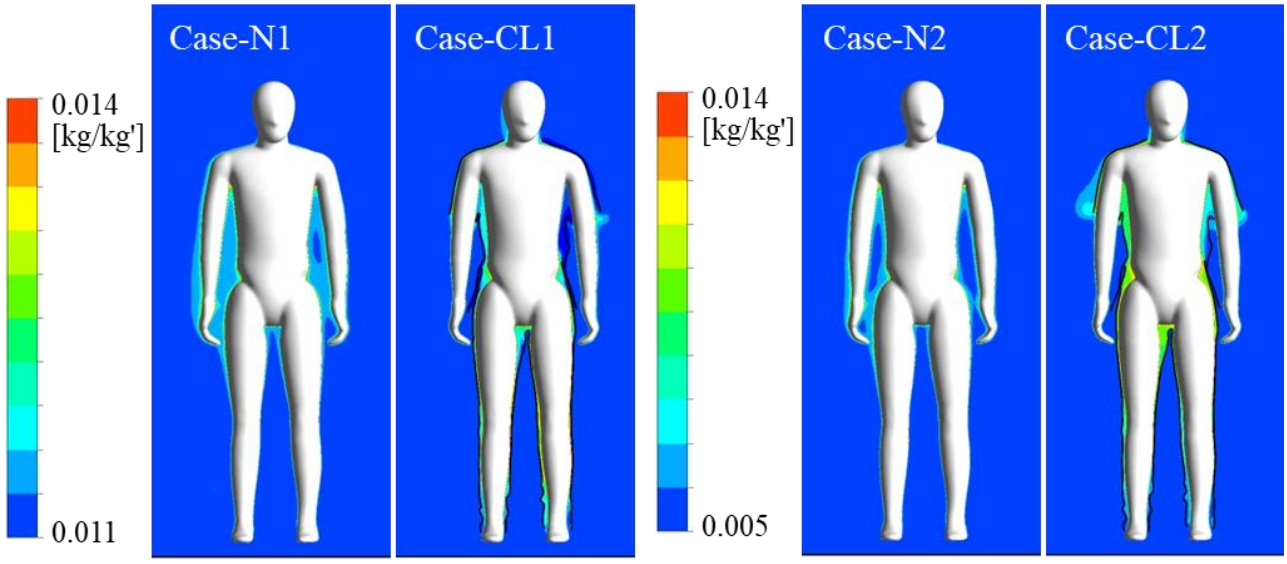

(b)

Figure 4-5. Temperature and humidity distribution around the human body for Case-N1, Case-N2, Case-CL1, and Case-CL2 at t = 600 s: (a) Temperature distribution and (b) Humidity distribution

These temperature results lead to an increase in skin surface temperature, as shown in Figure 4-6. Especially, a borderline on the mid-arm that showed a stark contrast in skin temperature between the clothed and exposed skin surface was clearly observed. Considering these thermoregulatory analyses under two types of thermal environmental conditions, the temperature filed around the CSP is directly in each skin temperature analysis result. A remarkable point was the smaller drop in the average skin temperature in the case of the naked model (4.1 °C) compared to the clothed one (3.1 °C) when the thermal environmental condition shifted from higher to low temperature.

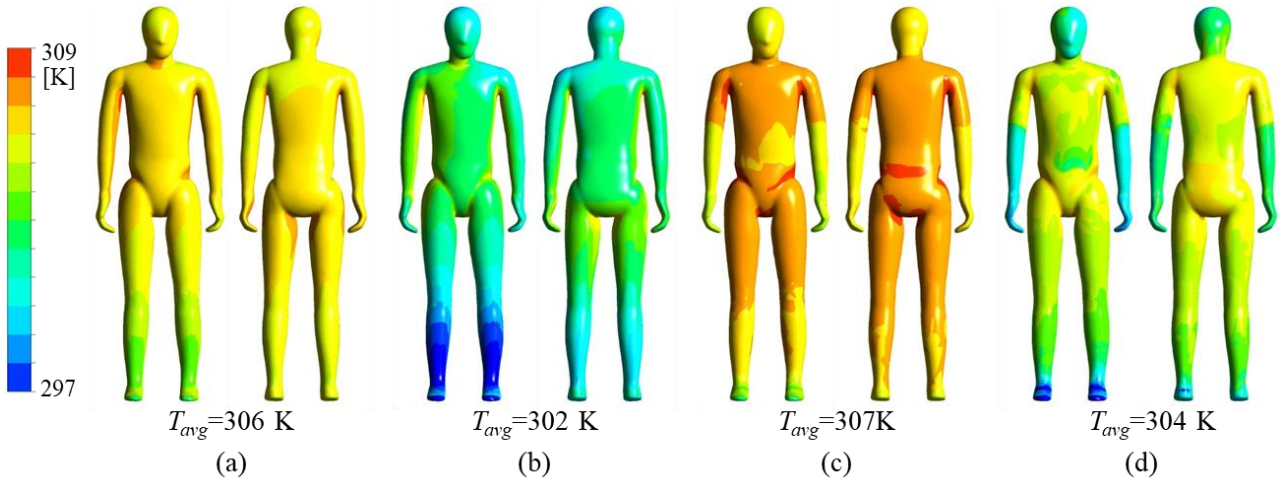

Figure 4-6. Temperature distribution on the human skin surface at t = 600 s: (a) Case-N1, (b) Case-N2, (c) Case-CL1, and (d) Case-CL2

The temperature distribution analysis results for the clothing surface is given in Figure 4-7, from which it can be observed that the clothing surface temperature was distributed based on the distance between the clothing and skin surface, which indicates the thickness of the thermal resistance layer. Meanwhile, a relatively lower temperature distribution was observed on the lower part of the pants due to a great deal of convective heat transfer under a strong flow filed around clothing, as the external environmental factor contributed to determining the clothing surface temperature.

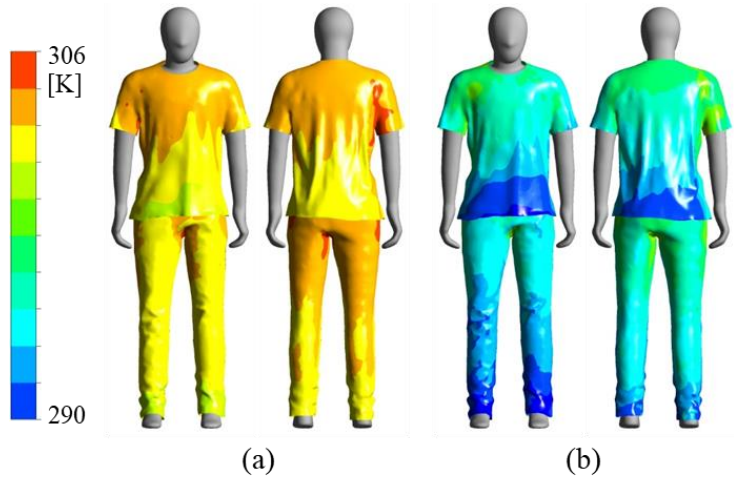

Figure 4-7. Temperature distribution on clothing surface at t = 600 s: (a) Case-CL1 and (b) Case-CL2

4.3.3 Formaldehyde concentration distribution

The formaldehyde concentration analysis results around CSP are summarized in Figure 4-8. The stagnant region in the center of the room is formed due to the layout of the inflow and outflow boundary, which assumes displacement ventilation, causing a higher formaldehyde concentration level around the CSP in most of the analytical cases. It is confirmed that velocity distribution higher than the velocity scale of molecular/turbulent diffusion has a dominant influence on the formation of concentration distribution; therefore, the formaldehyde concentration distribution is also in the transitional stage in the clothed model. Meanwhile, the change in location of the emission source caused different concentration levels in the indoor space.

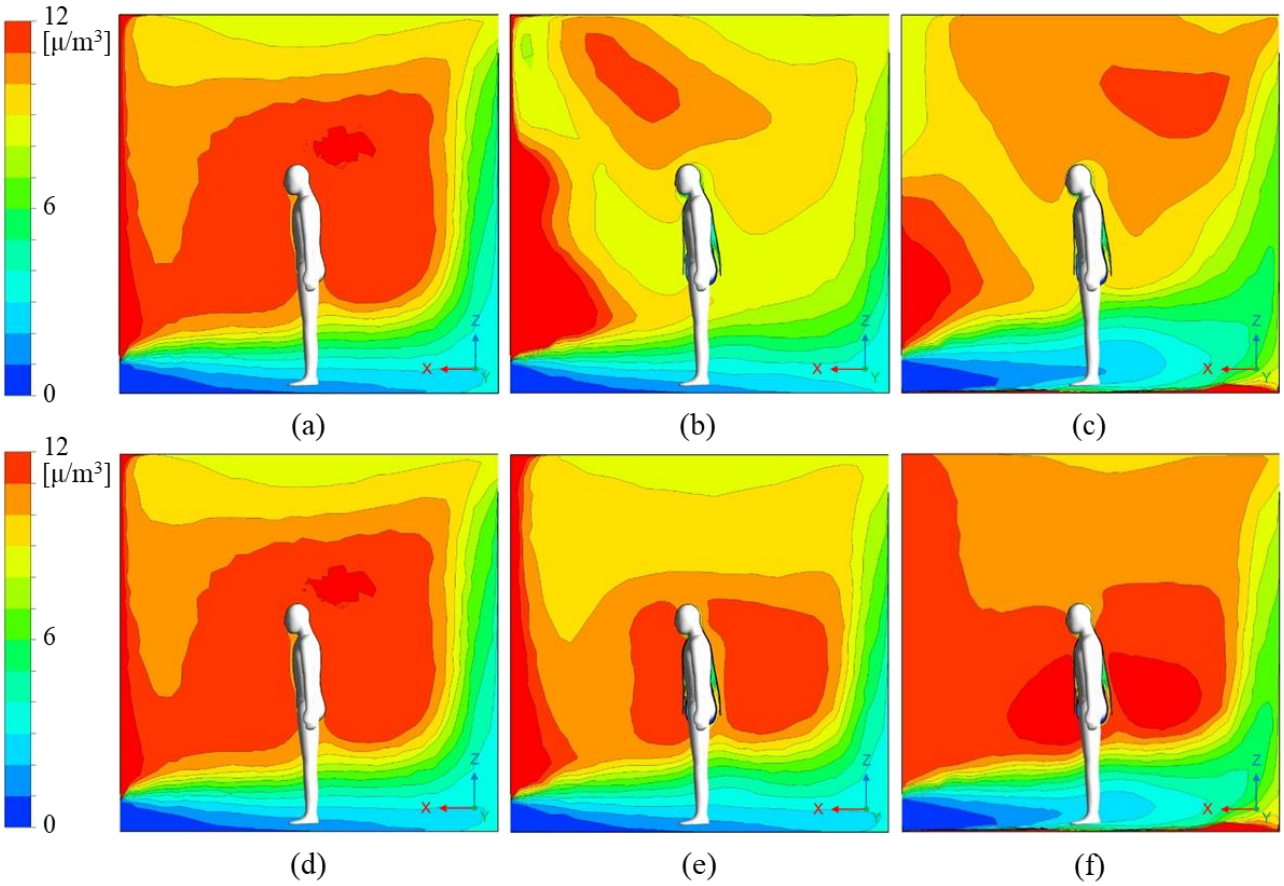

Figure 4-8. Formaldehyde concentration distribution for six cases: (a) Case-N1, (b) Case-CL1, (c) Case-CL3, (d) Case-N2, (e) Case-CL2, and (f) Case-CL4

As shown in Figure 4-9, higher volume-averaged indoor concentrations result in Case-CL3 and

Case-CL4 compared to the cases where the emission source is located as the CSP front wall. Formaldehyde, which reaches the clothing surface and is consistently adsorbed into clothing, leads to continuous concentration increase in clothing, as indicated in Figure 4-10.

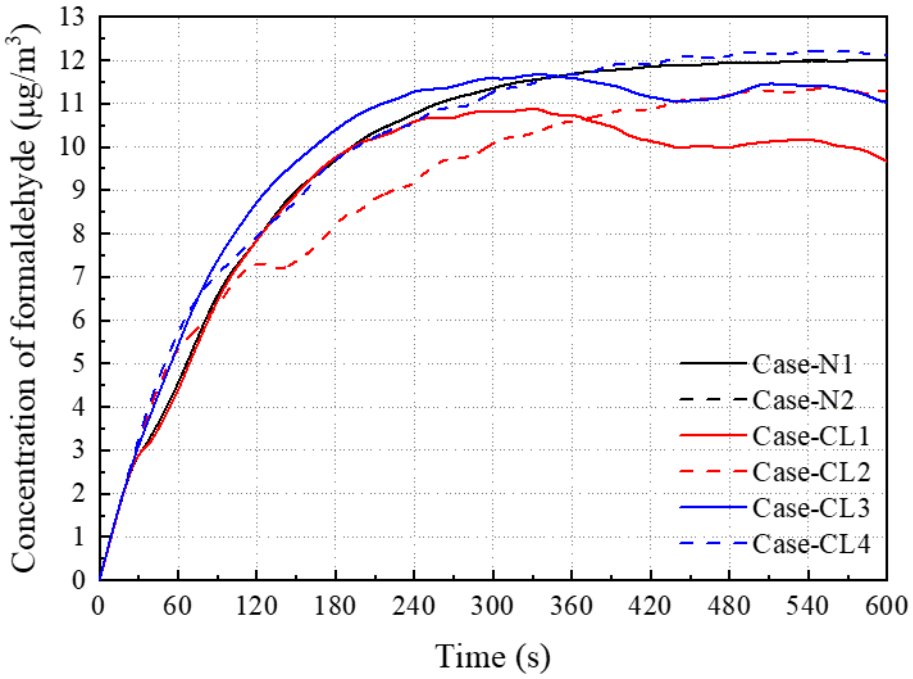

Figure 4-9. Time-series of volume-averaged formaldehyde concentration in indoor space for six cases

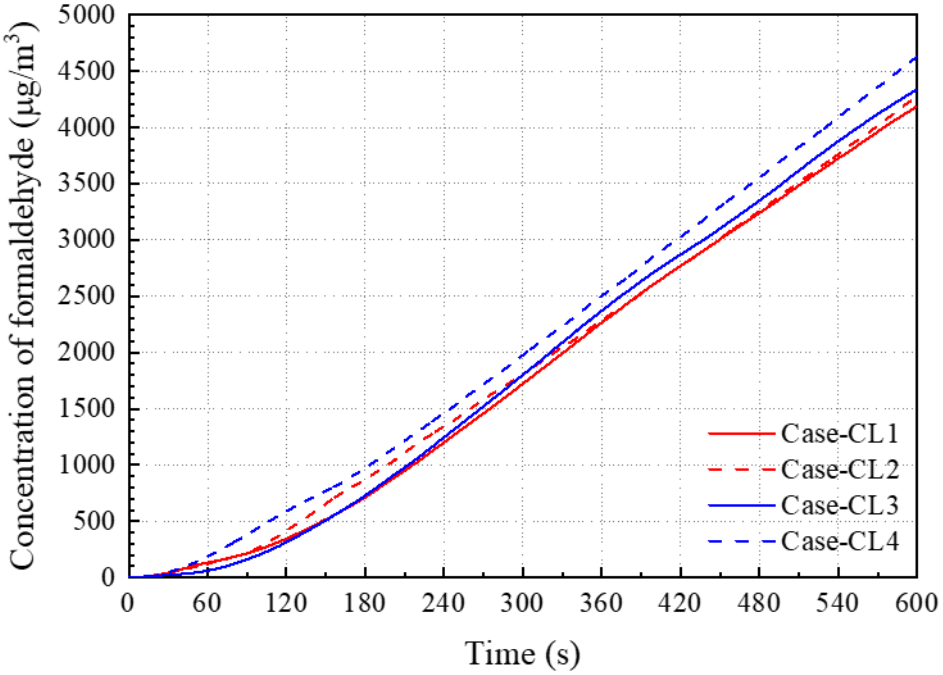

Figure 4-10. Time-series of volume-averaged formaldehyde concentration in inside clothing

4.3.4 Discussions

4.3.4.1 Clothing-focused analysis

The detailed investigation of the impact of clothing based on the indoor environmental factor suffers from a drawback, which can be summarized as the concentration distribution around the CSP or a volume-averaged concentration in indoor space. This section analyzed hygrothermal and formaldehyde concentration from the point of a certain distance ($y^+ < 30$ (buffer region; both viscous and turbulent shear dominates) from the clothing surface) to the skin surface, as shown in Figure 4-11. To check different airflow characteristics in the ventilation layer with different thicknesses, the analyses were positioned in two locations with 1.1 m and 1.4 m height, respectively.

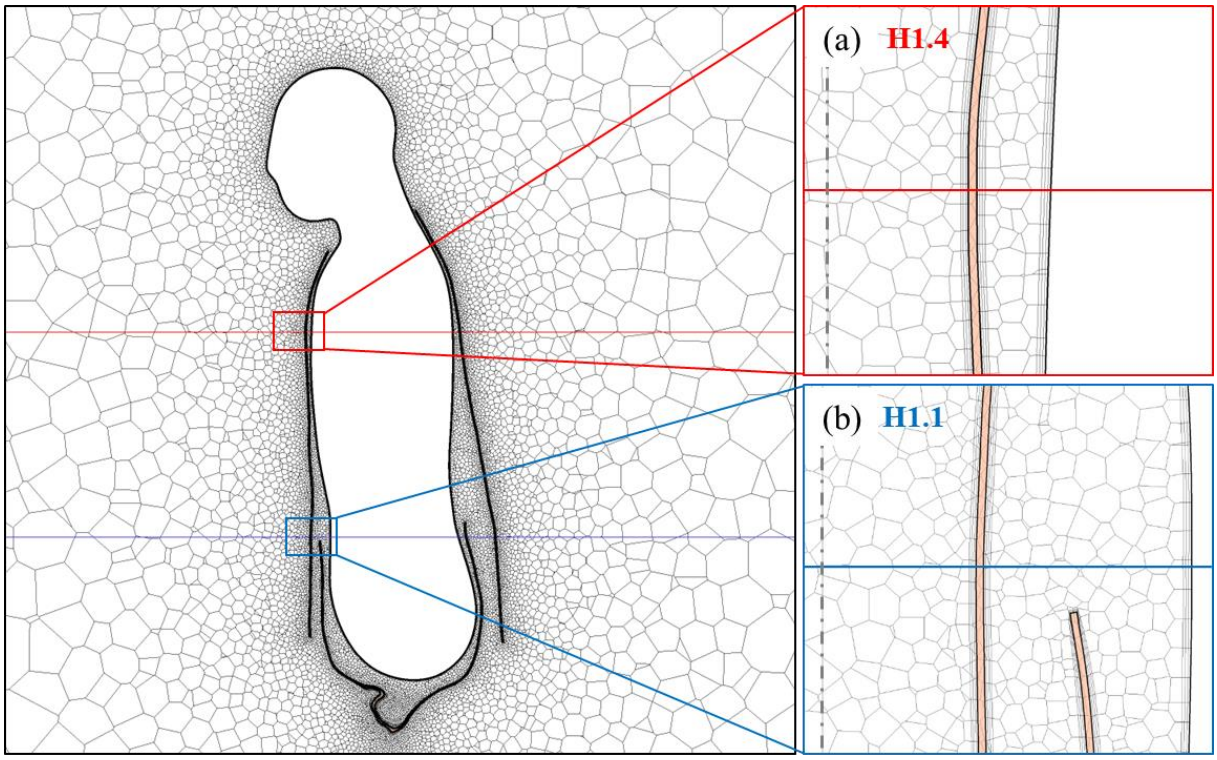

Figure 4-11. Outline of clothing-focused analysis at (a) H1.4 and (b) H1.1

The temperature at H1.4 and H1.1 are summarized in Figure 4-12. At location H1.4, the temperature of Caes-CL was 1 °C higher than that of Case-N due to the influence of clothing, while the tendency of temperature change was similar. At location H1.1, the velocity magnitude of the air gap between the clothing and skin surface was relatively low and the direction was varied, so the

temperature change showed a different trend compared to Case-N. As shown in Figure 4-13, the humidity change showed a similar trend to the temperature change, considering the initial condition of the humidity inside the clothing was dry.

The change in formaldehyde concentration at each location is indicated in Figure 4-14. The formaldehyde concentration of indoor space was higher in Case-CL3 and Case-CL4, where the emission source is located to the floor surface. In the cases with the clothed model, the difference in concentration depending on the supply temperature is precisely showed because of difference in buoyancy around CSP, whereas the difference due to temperature and location was insignificant in the cases with the naked model. In addition, the region at H1.4 where the temperature difference between clothing and skin surface in the air gap between clothing and skin increased, the formaldehyde concentration gradient on the skin surface increased in Case-CL2 and Case-CL4.

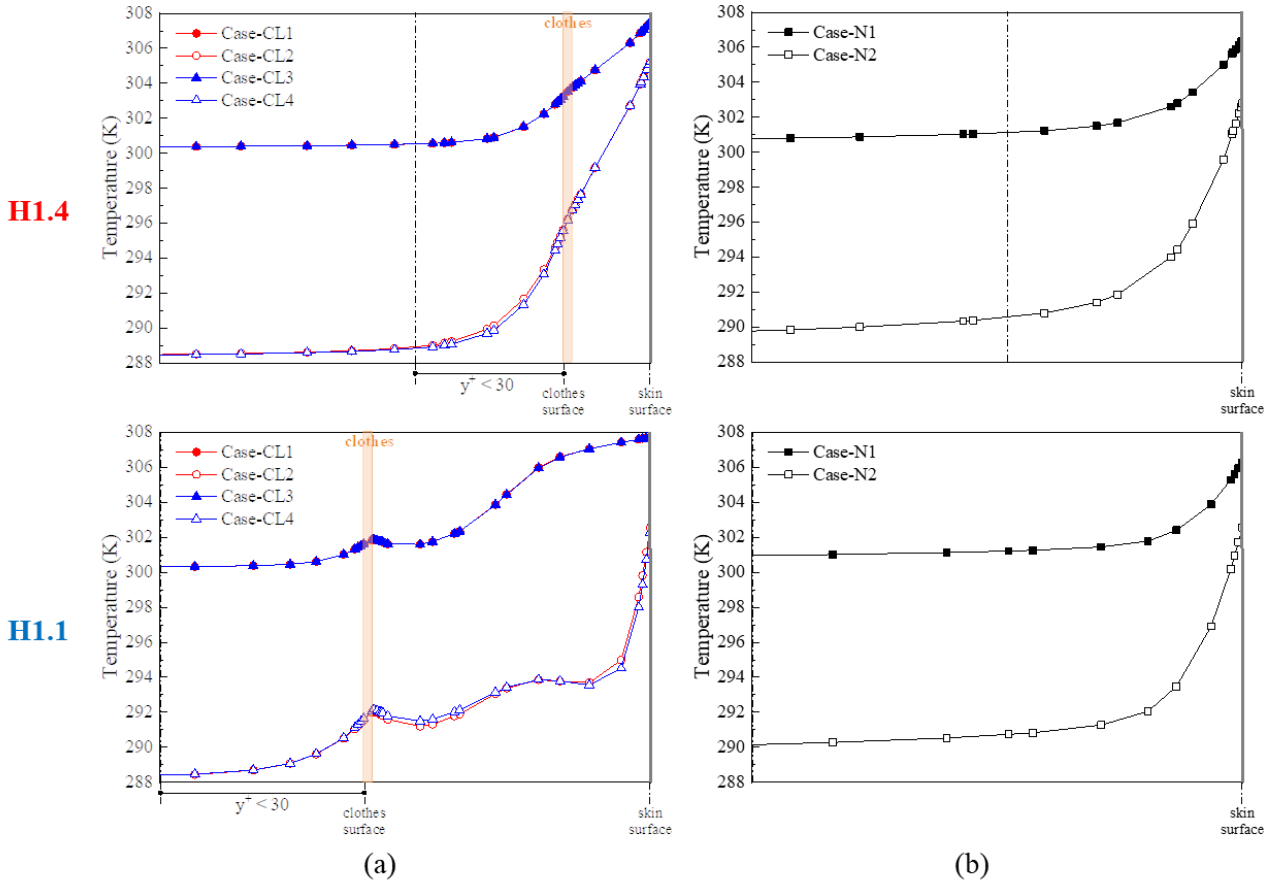

Figure 4-12. The temperature at H1.4 and H1.1: (a) Case-CL and (b) Case-N

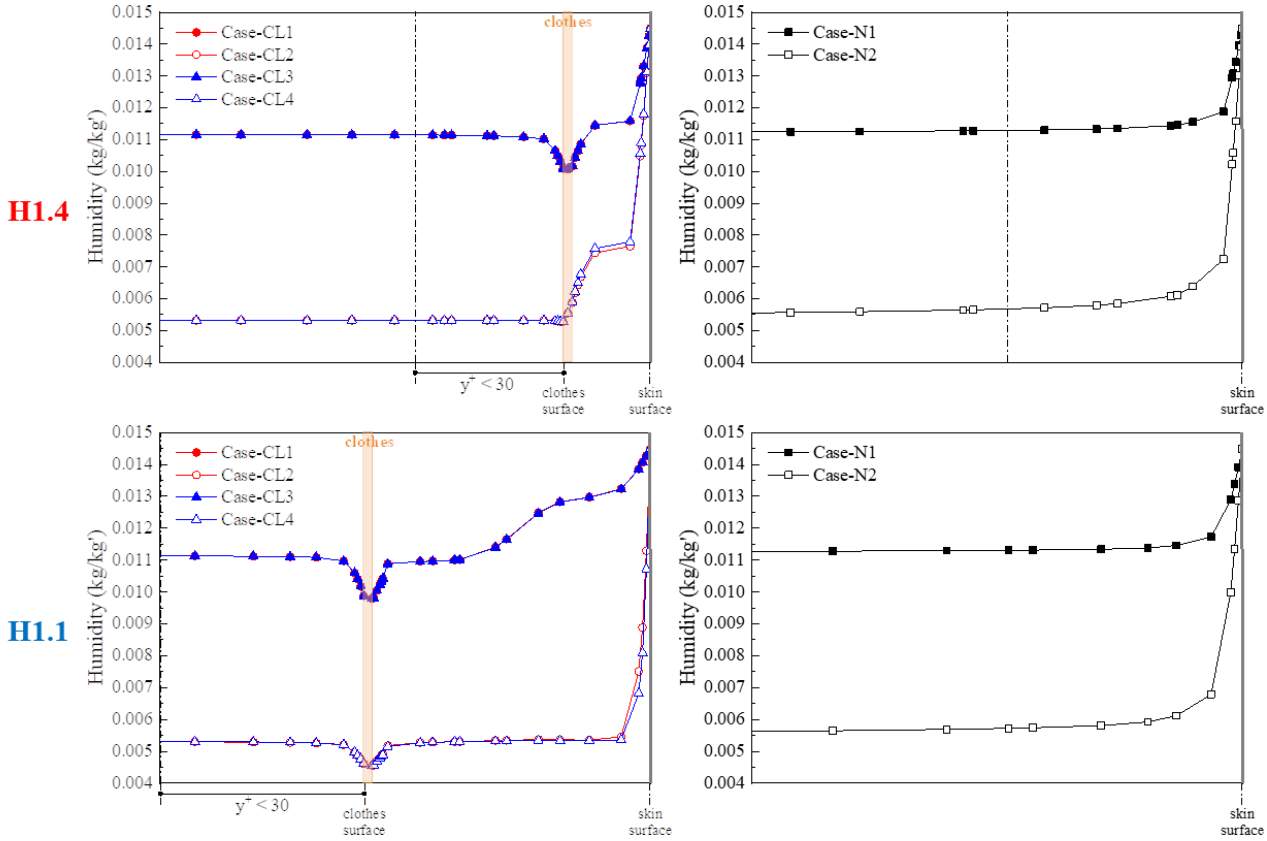

Figure 4-13. The humidity at H1.4 and H1.1: (a) Case-CL and (b) Case-N

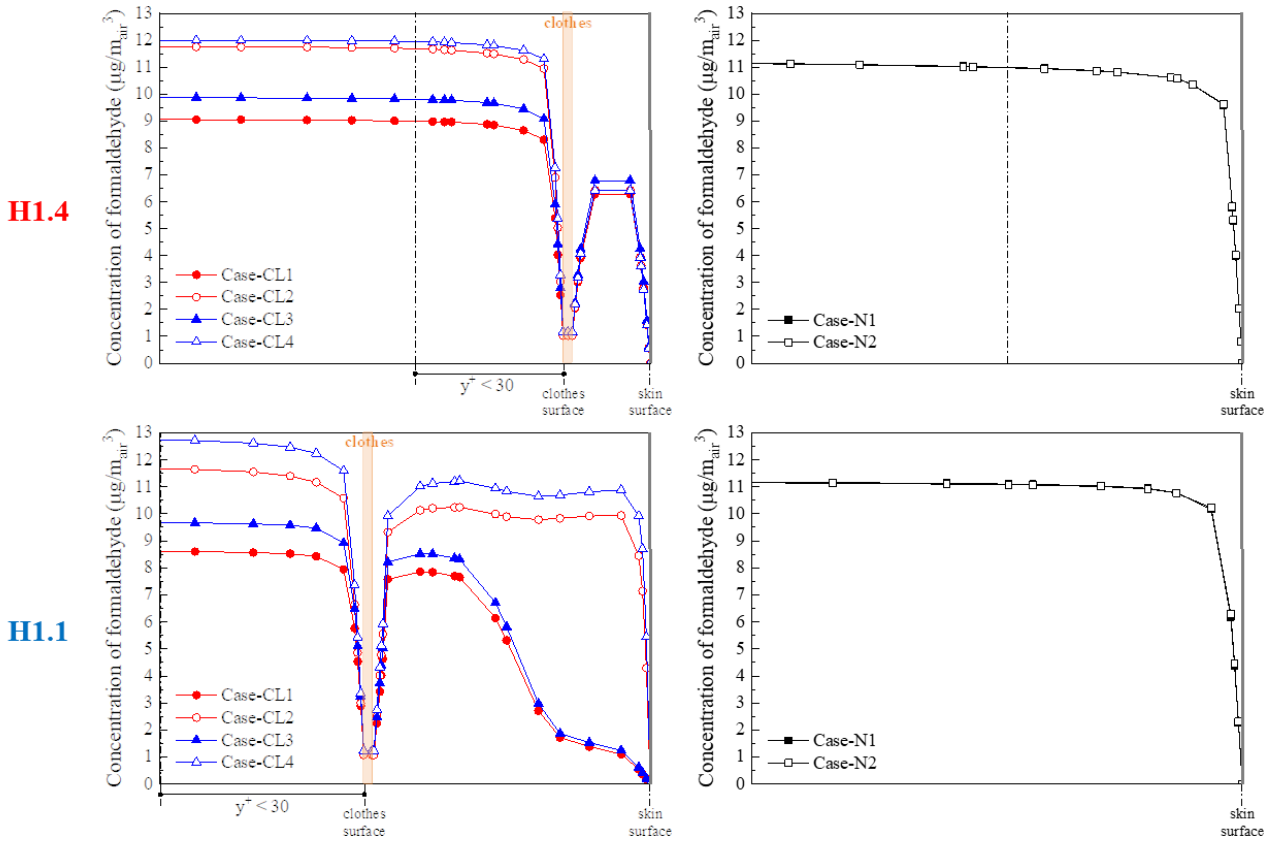

Figure 4-14. The formaldehyde concentration at H1.4 and H1.1: (a) Case-CL and (b) Case-N

An airflow field is formed in the air gap between clothing and skin, and the thermal environment in this space varies depending on the location of the reproduced clothing and supply temperature as shown in Figure 4-12. To quantitatively evaluate the change in heat/material transfer resistance according to the reproducibility of a detailed clothing model, the heat resistance around the human body for each ease is shown in Figure 4-15, representatively. As with the temperature change results, the heat resistance was different depending on the analysis location and temperature of the supply air. In the region where the ventilation layer is narrow, the difference in heat resistance due to changes in the thermal environment is insignificant. On the other hand, in the H1.1 location where the ventilation layer is wide, the difference in heat resistance according to the change in the thermal environment is largely affected by the indoor temperature since it is immediately after the inflow of indoor air. Moreover, compared to the heat resistance of Case-N1 and Case-N2 for the same distance, its values of Case-CL1 and Case-CL2 were more than twice as high. It is determined that these discussions for heat resistance, as well as detailed information on moisture and materials resistance, can be used as useful foundation data for establishing a simplified numerical model of clothing.

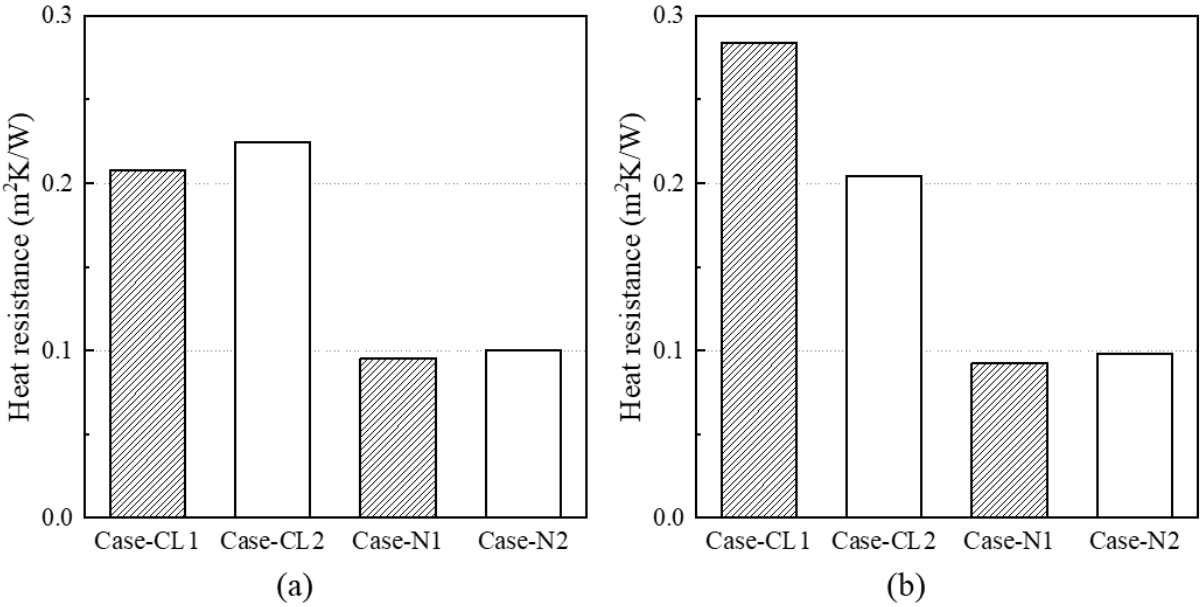

Figure 4-15. Heat resistance for six cases at (a) H1.4 and (b) H1.1

4.3.4.2 Risk of dermal exposure for formaldehyde

The complex flow field in the air gap (space between clothing and skin surface) with greater turbulent diffusion of contaminants can increase the risk of dermal exposure to chemical contaminants in indoor spaces, even though high ventilation performance may have some positive effects, especially on thermal comfort sensation.

The adsorption flux of formaldehyde on the skin surface for six cases is indicated in Figure 4-16. The analysis result of formaldehyde adsorption flux distribution on CSP showed that the flux distribution was affected by both airflow distribution and concentration distributions around CSP. In addition, the results of all cases with clothing demonstrated less adsorption flux overall, which indicated the impact of clothing on the dermal exposure to indoor contaminants as resistance to contaminant transfer.

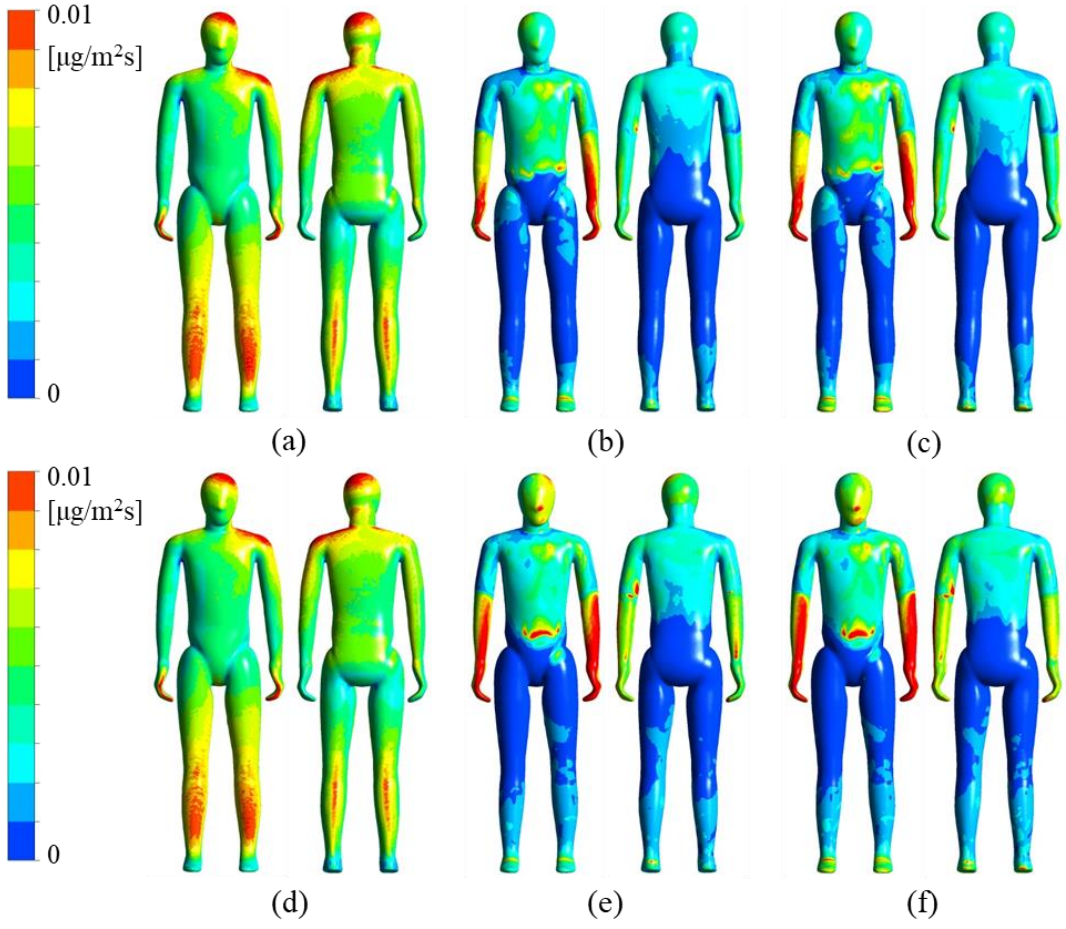

Figure 4-16. Adsorption flux of formaldehyde on the skin surface: (a) Case-N1, (b) Case-CL1, (c) Case-CL3, (d) Case-N2, (e) Case-CL2, and (f) Case-CL4

4.4 Limitation of this study

This study has several limitations. The integrated model of CSP with the clothed model used in this section reproduced a gap of at least 3 mm between clothing and skin on the whole surface of the human body, while the contacts between the clothing and skin surface were not reproduced because of technical limitations in grid generation. In fact, contact surfaces exist in some areas, such as the shoulders and upper chest, which causes the airflow to become blocked. Moreover, the thickness change of clothing was also ignored in this study.

To estimate human thermal sensation based on comprehensive CSP integrated with a detailed clothed model, the temperature on the surface of the human body is calculated using the 1-node thermoregulation model proposed by Fanger. This model is one of the basic and fundamental thermoregulation models, in which it is difficult to obtain detailed information regarding thermal comfort because of its simple modeling of the heat generated from the human body. In addition, the latent heat loss from the human body was reproduced using a boundary condition with fixed humidity. For advanced assessment, it is necessary to integrate multi-node and high-level human thermoregulation models, such as the Fiala or Stolwijk model, as one of our future tasks.

Regarding risk assessment of dermal exposure, perfect sink condition (C_{skin} = 0 μg/m^3), which assumes maximum adsorption, was used as the boundary condition of the skin surface. This technique corresponds to a ‘worst-case scenario,’ which is widely used to obtain overestimated exposure risk, and would be on the safe side for consideration. In future research, the physiologically based pharmacokinetic (PBPK) concept could be applied to improve the prediction accuracy of contaminant adsorption into human skin, which could allow us to obtain useful information regarding health risks such as saturable metabolism, reaction, and bold perfusion inside human skin.

4.5 Conclusion

In this chapter, an analysis model to analyze the transport of heat, moisture, and chemicals in the human-indoor environment system is developed. The analysis precision of the model was improved by integrating high-level models such as the multi-component molecular diffusion coefficient calculation and the hygrothermal transport models. In the analysis model, a CSP model integrated with the thermoregulation model was used to predict the impact of the human body.

Furthermore, to predict the influence of clothing on the analysis results, the development of a realistic clothing model based on 3D scanning techniques using real clothing with the establishment of a comprehensive estimation method of microclimate around clothing.

The airflow, hygrothermal, and chemical transfer analysis were conducted using the developed model for six cases concerning supply temperature and emission source location. As the results of numerical analysis, the reproducibility of the thermal resistance of clothing was confirmed based on thermoregulatory analysis with clothing. Moreover, the ventilation characteristics inside the air gap between the clothing and skin and contaminant exposure risk influenced by the indoor flow field and thermal environment were quantitatively estimated.

This study concluded that the proposed comprehensive estimation method could contribute to the investigation of more detailed characteristics of clothing microclimate, and clothing-centered interaction between humans and the surrounding environment.

CHAPTER 5

Conclusion

5.1 Summary

This study developed a numerical analysis model for hygrothermal (heat and moisture) and chemical transports in the human indoor environment system. To solve the transfer of airflow, heat, moisture, and chemicals existing in the indoor environment, the focus was on the numerical analysis method using fluid dynamics CFD simulation. Regarding the analysis model, a high-precision analysis model was prepared using high-level models such as a multi-component diffusion coefficient model and a hygrothermal transfer model, to increase the precision of numerical analysis reproducing the transport phenomenon model. The present research focused on formaldehyde, a common and major pollutant in building materials, to analyze the diffusion of chemicals.

A summary of each chapter is presented:

Chapter 1 summarized the introduction of the present research. It focuses on the necessity of developing a numerical analysis model that considers the interaction of each factor in the heat and moisture transports and chemical transport to predict IAQ. Furthermore, an advanced CSP model capable of dealing with specific characteristics of the human body that reproduces the detailed clothing shapes have also been discussed.

Chapter 2 described the fundamental mathematical models that describe the physical characteristics of airflow, thermal, humidity, and chemical transports through equations. It is explained based on the CFD simulation. Furthermore, chemical emission mechanism from building materials was described, and the diffusion characteristics by indoor environment parameters in gas and liquid phases were introduced. Especially, a multi-component diffusion coefficient model that calculates the diffusion coefficient of a target substance in mixed air containing moisture or other

chemicals was described.

Chapter 3 summarized the emission rates of chemicals from building materials and concentration distribution formation in a confined desiccator under isothermal condition. Here, the analysis conditions reproduce the molecular diffusion dominated environmental system.

In the environment considering only molecular diffusion, it was confirmed through numerical analysis the diffusion phenomenon of chemical presents differently according to the shape of the diffusion field; especially, there was a significant difference in the case of external/evaporative diffusion control type that assumes the emission concentration from building material is fixed. A parameter, equivalent diffusion length (L_d), was proposed as a method to correct the different results for emission rates by the desiccator geometry, and its usefulness was confirmed based on numerical analysis using this parameter.

Chapter 4 summarized the development of an integrated numerical model in human-indoor environmental to analyze the hygrothermal and chemical transports. In addition, the change in temperature, humidity, and contaminant concentration in the air gap between the clothing and skin surface was estimated using the CSP with the clothed model.

The thermal resistance of clothing was confirmed based on the result of temperature distributions. Moreover, the change of airflow in the indoor space and the ventilation characteristics of the air gap between the clothing and skin surface was confirmed by reproducing the clothing model. The exposure risk of contaminant influence by the indoor flow field and the thermal environment was quantitatively estimated in this chapter.

Furthermore, parametric analyses were performed to investigate the impact of indoor environmental factors such as indoor temperature and emission source location; as a result, it is confirmed that the temperature of the supply air influences the concentration of contaminants near the CSP with the clothed model and the exposure risk of the human body.

5.2. Future works

The present research presented techniques to reproduce the transport of hygrothermal and chemicals in the human indoor environment. The final aim of this study is the modeling of numerical analysis to predict the concentration distribution of chemicals in indoor environments in considering the simultaneous transport phenomenon of heat and moisture. Future work has been planned, as described below.

1. Since only the adsorption of formaldehyde was performed for a short period of 10 minutes, it is necessary to confirm the desorption phenomenon in clothes and the delay of human exposure time after removing the contaminants. The airflow was not stabilized by the complicated shape of the clothes; therefore, sufficient time is required for calculation. It was not determined but theoretically is expected to take approximately 2 hours by the adsorption phenomenon in the clothes.

2. For advanced assessment, it is necessary to integrated multi-node and high-level human thermoregulation models, such as the Fiala or Stolwijk model. Moreover, to improve the prediction accuracy of contaminant adsorption into human skin, the boundary condition of the skin surface is applied based on the measurement results of previous researches on the contaminant adsorption of the dermal surface.

3. The human body and clothing models are 3D scanning data based on real thermal manikin and clothes. For the analysis in various indoor environments, the CSP has to be developed and simplifies by developing a numerical model based on the calculation results of this study.

REFERENCES

[1] Nmieśnik, J., Górecki, T., Kozdroń-Zabiegała, B., Łukasiak, J. (1992). Indoor air quality (IAQ), pollutants, their sources and concentration levels. *Build Environ*, 27, 339-356.

[2] Russell, J.A., Hu, Y., Chau, L., Pauliushchyk, M., Anastopoulos, I., Anandan, S., Waring, M.S. (2014). Indoor-Biofilter Growth and Exposure to Airborne Chemicals Drive Similar Changes in Plant Root Bacterial Communities. *Appl Environ Microbiol*, 80 (16), 4805-4813.

[3] Murakami, S. (2004). Analysis and design of micro-climate around the human body with respiration by CFD. *Indoor Air*, 14, 144-156.

[4] Murakami, S., Kato, S., Zeng, J. (2000). Combined simulation of airflow, radiation and moisture transport for heat release from human body. *Build Environ*, 35, 489-500.

[5] Ito, K. (2014). Integrated numerical approach of CFD and epidemiological model for multi-scale transmission analysis in indoor spaces. *Indoor Built Environ*, 23 (7), 1029-1049.

[6] Nakahara, K., Yamaguchi, T., Lim, E., Ito, K. (2017). Computational fluid dynamics modeling and parameterization of the visible light photocatalytic oxidation process of toluene for indoor building material. *Sustain Cities Soc*, 35, 298-308.

[7] Murga, A., Yoo, S. J., Ito, K. (2016). Multi-stage downscaling procedure to analyze the impact of exposure concentration in a factory on a specific worker through CFD. *Indoor Built Environ*, 27, 486-498.

[8] Lim, E., Chung, J., Sandberg, M., Ito, K. (2010). Influence of chemical reactions and turbulent diffusion on the formation of local pollutant concentration distributions, Chem Rev, 110 (4) 2536-2572.

[9] Spengler, J.D., Chen, Q. (2000). Indoor air quality factors in designing a healthy building. *Annu Rev Energ Env*, 25 (1), 567-600.

[10] Wang, C., Yoo, S., Tanabe, S., Ito, K. (2020). Investigation of transient and heterogeneous micro-climate around a human body in an enclosed personalized work environment. *Energy and Built Environment*, 1, 423-431.

[11] Murga, A., Long, Z., Yoo, S., Sumiyoshi, E., Ito, K. (2020). Decreasing inhaled contaminant dose of a factory worker through a hybrid Emergency Ventilation System: performance evaluation in worst-case scenario. *Energy and Built Environment*, 1, 319-326.

[12] Yoo, S., Ito, K. (2018). Numerical prediction of tissue dosimetry in respiratory tract using computer simulated person integrated with physiologically based pharmacokinetic–computational fluid dynamics hybrid analysis. *Indoor Built Environ*, 27 (7), 877-889.

[13] Yoo. S., Ito, K. (2018). Assessment of transient inhalation exposure using in silico human model integrated with PBPK - CFD hybrid analysis. *Sustain Cities Soc*, 40, 317-325.

[14] Phuong, N.L., Yamashita, M., Yoo, S., Ito, K. (2016). Prediction of convective heat transfer coefficient of human upper and lower airway surfaces in steady and unsteady breathing conditions. *Build Environ*, 100, 172-185.

[15] Phuong, N.L., Khoa, N.D., Ito, K. (2020). Comparative numerical simulation of inhaled particles dispersion in upper human airway for inter-subject differences. *Indoor Built Environ*, 29 (6), 793-809.

[16] Wang, C., Yoo, S., Ito, K. (2019). Does detailed hygrothermal transport analysis in respiratory tract affect skin surface temperature distributions by thermoregulation model?. *Advances in Building Energy*. 1-21.

[17] Kuga, K., Ito, K., Yoo, S. J., Chen, W., Wang, P., Liao, J., Fowles, J., Shusterman, D., Kumagai, K. (2018). First-and second-hand smoke exposure assessment from e-cigarettes using integrated numerical analysis of CFD and a computer-simulated person with a respiratory tract model. *Indoor Built Environ*, 27, 898-916.

[18] Kuga, K., Ito, K., Chen, W., Wang, P., Kumagai, K. (2020). A numerical investigation of the potential effects of e-cigarette smoking on local tissue dosimetry and the deterioration of indoor air quality. *Indoor Air*.

[19] Zhang, J.S. (2005). Combined Heat, Air, Moisture, and Pollutants Transport in Building Environmental System. *JSME Int J*, 48 (2), 182-190.

[20] Fiala, D., Lomas, K.J., Stohrer, M., (1999). A computer model of human thermoregulation for a wide range of environmental conditions: the passive system. *J Appl Physiol*, 87 (5), 1957-1972.

[21] Fiala, D., Havenith, G., Br€ode, P., Kampmann, B., Jendritzky, G. (2012). UTCI-Fiala multi-node model of human heat transfer and temperature regulation. *Int J Biometeorol*, 56 (3), 429-441.

[22] Smith, C.E. (1991). A transient, three-dimensional model of the human thermal system (Ph.D. thesis). Kansas State University, Manhattan, United States.

[23] Stolwijk, J.A.J. (1971). A Mathematical Model of Physiological Temperature Regulation in Man. NASA Technical Report NASA CR-855.

[24] Tanabe, S., Kobayashi, K., Nakano, J. (2002). Evaluation of thermal comfort using combined multi-node thermoregulation (65MN) and radiation models and computational fluid dynamics (CFD). *Energy Build*, 34 (6), 637-646.

[25] Takada, S., Sasaki, A., Kumura, R. (2016). Fundamental study of ventilation in air layer in clothing considering real shape of the human body based on CFD analysis. *Build Environ*, 99, 210-220.

[26] Murakami, S., Kato, S., Chikamoto, T., Laurence, D., Blay, D. (1996). New Low-Reynolds-Number k-ε model including damping effect due to Buoyancy in a stratified Flow Field. *Int J Heat Mass Transfer*, 39 (16), 3483-3496.

[27] Gosselin, J.R., Chen, Q.Y. (2008). A computational method for calculating heat transfer and airflow through a dual-airflow window. *Energy Build*, 40, 452-458.

[28] Chung, J., Sotokawa, H., Kameishi, K., Yoo, S., Ito, K. (2019). Performance Evaluation of Heat Exchange Element by Numerical Model, Part 2 – Heat and Mass Transfer Analysis in

Energy Recovery Ventilator by Coupled CFD and Hygrothermal Transfer Model. Trans Soc Heating Air Condit Sanit Eng Jpn, 271, 1-9. (in Japanese)

[29] Ito, K., Takigasaki, K. (2011). Multi-target identification for emission parameters of building materials by unsteady concentration measurement in airtight micro-cell-type chamber. *Build Environ*, 46 (2), 518-526.

[30] Zhu, Q., Kato, K., Murakami, S., Ito, K. (2007). 3D-CFD analysis of diffusion and emission of VOCs in a FLEC cavity. *Indoor Air*, 17 (3), 178-188.

[31] Ito, K., Tanabe, S., Kumagai, K. (2006). Numerical analysis of diffusion fields in passive type flux sampler and estimation of effective diffusion length. *J Environ Eng*, 71 (603), 47-54. Transactions of AIJ (Japanese)

[32] Murakami, S., Kato, S., Ito, K. (1998). Coupled analysis of TVOC emission and diffusion in ventilated room by CFD. *EPIC*, 1, 19-26.

[33] Que, Z., Furuno, T. (2007). Formaldehyde emission from wood products: relationship between the values by the Chamber method and those by the Desiccator test. *Wood Sci Technol*, 41, 267-279.

[34] Yang, X., Chen, Q., Bluyssen, P.M. (1998). Prediction of short-term and long-term VOC emissions from SBR bitumen-backed carpet under different temperatures. Atlanta: ASHRAE Transactions, vol. 104, pp. 1297

[35] Little, J.C., Hodgson, A.T., Gadgil, A.J. (1994). Modeling emissions of volatile organic compounds from new carpets. *Atmos Environ*, 28, 227-234.

[36] Hoetjer, J.J., Koerts, F. (1986). *A model for formaldehyde release from particleboard*. In: Meyer B, Kottes Andrew BA, Reinhardt RM (eds) Formaldehyde release from wood products. Washington: ACS, pp. 125-144.

[37] Fairbanks, D.F., Wilke, C.R. (1950). Diffusion Coefficients in Multicomponent Gas Mixtures. *Ind Eng Chem*, 42 (3), 471-475.

[38] Wilke, C.R. (1950). *Diffusional properties of multicomponent gases*. In: Chemical Engineering Progress, vol. 46, pp. 95-101.

[39] ISO 16000-9. (2006). Part 9: determination of the emission of volatile organic compounds from building products and furnishing – emission test chamber method. Geneva: The International Organization for Standardization.

[40] Brown, S.K. (1999). Chamber assessment of formaldehyde and VOC emissions from wood-based panels. Indoor Air, 9, 209.

[41] Yu, C.W.F., Crump, D. (1999). Testing for formaldehyde emission from wood-based products – a review. Indoor Built Environ, 8, 280-374.

[42] JIS A 1460. (2001). Building Boards. Determination of Formaldehyde Emission – Desiccator Method. Tokyo: Japanese Industrial Standard.

[43] ISO/DIN 12460-4. (2016). Wood-based panels – determination of formaldehyde release – part 4: desiccator method. Berlin: Deutsches Institut für Normung.

[44] Risholm-Sudman, M., Larsen, A., Vestin, E., Weibull, A. (2007). Formaldehyde emission – Comparison of different standard methods. *Atmos Environ*, 41 (15), 3193-3202.

[45] Kim, S., Kim, J., Kim, H., Kim, S. (2006). Determination of formaldehyde and TVOC emission factor from wood-based composites by small chamber method. *Polym Test*, 25(5), 604-614.

[46] Que, Z., Furuno, T. (2007). Formaldehyde emission from wood products: relationship between the values by the Chamber method and those by the Desiccator test. *Wood Sci Technol*, 41, 267-279.

[47] Que, Z., Wang, F., Ma, L., Furuno, T. (2013). Effect of loading ratio, conditioning time and air exchange rate on the formaldehyde emission from wood-based board using large chamber and desiccator method. *Compos B Eng*, 47, 278-282.

[48] Böhm, M., Salem, M.Z.M., Srba, J. (2012). Formaldehyde emission monitoring from a variety of solid wood, plywood, blockboard and flooring products manufactured for building and furnishing material. J Hazard Mater, 221-222, 68-79.

[49] Japan Testing Center for Construction Materials (JTCCM). (2019). Report on the Development of Japanese Industrial Standard – Determination of the Emission of Formaldehyde from Building Boards – Desiccator Method.

[50] ISO 13130. (2011). Laboratory glassware – desiccators. Geneva: The International Organization for Standardization. *Sustain Cities Soc*, 40, 317-325.

[51] Sander, R. (2015). Compilation of Henry's law constant (version 4.0) for water as solvent. *Atmos Chem Phys*, 15, 4399-4981.

[52] Warneck, P., Williams, J. (2012). The atmospheric chemist's companion. Dordrecht: Springer.

[53] Ito, K. (2013). Integrated numerical simulation with fungal spore deposition and subsequent fungal growth on bathroom wall surface. *Indoor Built Environ*, 22 (6), 881-896.

[54] Kaden, D.A., Mandin, C., Nielsen, G.D., Wolkoff, P. (2010). *Formaldehyde*. In: WHO guideline for indoor air quality: selected pollutants. Geneva: World Health Organization, pp. 140-142.

[55] Braswell, J.R., Spiner, D.R., Hoffman, R.K. (1970). Adsorption of Formaldehyde by Various Surface During Gaseous Decontamination. *Appl Microbiol*, 20(5), 765-769.

[56] Rowen, J.W., Blaine, R.L. (1947). Sorption of Nitrogen and Water Vapor on Textile Fibers. *J Res Bur Stand*, 39, 497-486.

[57] Foat, T.G., Parker, S.T., Castro, I.P., Xie, Z.T. (2018). Numerical investigation into the structure of scalar plumes in a simple room. *J Wind Eng Ind Aerod*, 175, 252-263.

[58] Ito, K., Inthavong, K., Kurabuchi, T., Ueda, T., Endo, T., Omori, T., et al. (2015). CFD benchmark tests for indoor environmental problems: part 1 isothermal/non-isothermal flow in 2D and 3D room model. *Journal of Architectural Engineering Technology*, 2 (1), 1-22.

[59] Ito, K., Inthavong, K., Kurabuchi, T., Ueda, T., Endo, T., Omori, T., et al. (2015). CFD benchmark tests for indoor environmental problems: Part 2 cross-ventilation airflows and floor heating systems. *Journal of Architectural Engineering Technology*, 2 (1), 23-49.

[60] Ito, K., Inthavong, K., Kurabuchi, T., Ueda, T., Endo, T., Omori, T., et al. (2015). CFD benchmark tests for indoor environmental problems: part 3 numerical thermal manikins. *Journal of Architectural Engineering Technology*, 2 (1), 50-75.

[61] Ito, K., Inthavong, K., Kurabuchi, T., Ueda, T., Endo, T., Omori, T., et al. (2015). CFD benchmark tests for indoor environmental problems: part 4 air-conditioning airflows, residential kitchen airflows and fire-induced flow. *Journal of Architectural Engineering Technology*, 2 (1), 76-102.

[62] Nielsen, P.V. (1990). Specification of a two-dimensional test case: (IEA) , Vol. 1 (No. 8, Aalborg: Institut for Bygningsteknik, Aalborg UniversitetR9040 [Gul serie].

[63] Nielsen, P.V. (2015). Fifty years of CFD for room air distribution. *Build Environ*, 91, 78-90.

[64] Sorensen, D.N., Nielsen, P.V. (2003). Quality control of computational fluid dynamics in indoor environments. *Indoor Air*, 13, 2-17.

[65] Patankar, S.V. (1980). Numerical heat transfer and fluid flow. McGraw-Hill International Book Co.

[66] Ke, Y., Li, J., Hvenith, G. (2014). An improved experimental method for local clothing ventilation measurement. *Int J Ind Ergon*, 44, 75-81.

[Previously published documents related the present research]

[1] Kang, Y., Yoo, S., Takenouchi, K., Yoshida, H., Tanabe, S., Ito, K. (2019). Distribution of transient formaldehyde concentration in confined small glass desiccators and its impact on emission rate measurement. *Atmos Environ*, 218, 116979.

[2] Kang, Y., Yoo, S., Ito, K. (2020). Correlation between formaldehyde emission characteristics in enclosed desiccators with five different geometries. *Indoor Built Environ*, DOI: 10.1177/1420326X20908918

[3] Kang, Y., Murota, K., Hyodo, S., Yoo, S., Takenouchi, K.,Tanabe, S., Ito, K. 3D digital Clothing Model Integrated with Computer-Simulated Person and Comprehensive Analysis of Clothing Microclimate. *Build Environ*, Submitted.